






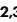


Epigenetic adaptation of beta cells across lifespan and disease

Received: 1 July 2025

Accepted: 2 March 2026

Published online: 24 April 2026


 Check for updates

Elisabetta Manduchi ^{1,2,3}, H el ene C. Descamps ^{1,2,3}, Jinping Liu^{1,2,3}, Jonathan Schug^{1,2,3}, Tong Da^{1,2,3}, Deeksha Lahori^{1,2,3}, Hilana El-Mekkoussi^{1,2,3}, Michelle Lee^{1,2,3}, Eseye Feleke^{4,5}, Diana Bernstein^{1,2}, Chengyang Liu ^{3,6}, Ali Naji^{3,6}, Benjamin Glaser ⁵, Klaus H. Kaestner ^{1,2,3}  & Dana Avrahami ^{4,5} 

Although the prevalence of type 2 diabetes (T2D) increases with age, most adults maintain normoglycaemia despite rising insulin resistance owing to the adaptive capacity of pancreatic beta cells to meet increased metabolic demand. However, persistent insulin resistance can lead to beta cell dysfunction and T2D onset. Here we show the mapping of genome-wide DNA methylation (DNAm) patterns and the epigenomic basis of beta cell adaptations by leveraging cell-type-specific methylome data from the Human Pancreas Analysis Program. In healthy donors, we identify progressive age-related demethylation enriched in *cis*-regulatory elements at beta cell identity and function genes. By contrast, alpha cells show the opposite trajectory, with subtle, age-related hypermethylation. In T2D beta cells, but not alpha cells, we observed further demethylation compared to healthy controls, underscoring a unique capacity of beta cells to respond to changes in metabolic demand. Together, our findings suggest that DNAm remodelling in healthy beta cells reflects a long-term adaptation to metabolic demand, which, in T2D, is accelerated as part of a compensatory response that ultimately fails under sustained insulin resistance.

Ageing is commonly described as the gradual decline in physiological functions and metabolic regulation, a process observed across the animal kingdom. However, although physiological deterioration predominantly occurs in the later stages of life, recent studies suggest that the ageing process can also include phases of physiological adaptation and even functional improvement. During human adulthood, many physiological functions remain stable for decades, reflecting ongoing adaptation. For instance, older adults maintain the ability to improve cardiovascular fitness and cardiac output in response to aerobic exercise¹, enhance endothelial function to reduce arterial stiffness² and sustain daily energy expenditure³.

Pancreatic beta cells have a crucial role in regulating glucose homeostasis by secreting insulin in response to elevated blood glucose levels. Failure to adequately compensate for insulin resistance can lead to persistent hyperglycaemia and, eventually, T2D⁴. Although insulin resistance and elevated blood glucose levels tend to worsen with age^{4–6}, most older individuals maintain normoglycaemia. This suggests that beta cells, which are long-lived and rarely proliferate in adulthood^{7–10}, must sustain function over decades by continually adapting to fluctuating metabolic demands. Indeed, beta cells can adapt during physiological insulin-resistant states, such as pregnancy and puberty, by expanding their mass and enhancing their capacity to

¹Institute of Diabetes, Obesity, and Metabolism, Perelman School of Medicine, The University of Pennsylvania, Philadelphia, PA, USA. ²Department of Genetics and Institute for Diabetes, Obesity, and Metabolism, University of Pennsylvania Perelman School of Medicine, Philadelphia, PA, USA. ³The Human Pancreas Analysis Program (RRID:SCR_016202), Philadelphia, PA, USA. ⁴Department of Developmental Biology and Cancer Research, The Hebrew University Hadassah Medical School, Jerusalem, Israel. ⁵Department of Endocrinology and Metabolism, Hadassah Medical Center, Faculty of Medicine, Hebrew University of Jerusalem, Jerusalem, Israel. ⁶Department of Surgery and Institute for Diabetes, Obesity, and Metabolism, Perelman School of Medicine, University of Pennsylvania, Philadelphia, PA, USA.  e-mail: kaestner@upenn.edu; dana.tzfati@mail.huji.ac.il

secrete insulin^{11,12}. Our prior transcriptomic analysis of human beta cell ontogeny supports the notion that beta cells activate genes critical to their function to sustain enhanced activity with age¹³. This finding is further corroborated by a recent report¹⁴ that highlights a beneficial adaptive response in beta cells throughout adulthood, associated with enhanced glucose-stimulated insulin secretion (GSIS), that persists at least until age 60 (ref. 14).

DNAm, a relatively stable epigenetic mark, exhibits cell-specific patterns in regulatory regions, helping to maintain cell-type-specific expression programmes across multiple cell generations and throughout life¹⁵. Despite its stability, DNAm patterns are altered gradually over the human lifespan, with changes at specific sites serving as an epigenetic clock and providing one of the most accurate predictors of chronological age¹⁶. Although numerous studies have shown DNAm alterations in the context of cancer¹⁷, far fewer have explored how factors related to metabolic diseases impact DNAm and, more specifically, how these methylation changes may contribute to the development of T2D. Previous studies have reported DNAm alterations in the promoters and enhancers of genes associated with insulin secretion in whole islets of deceased organ donors with T2D^{18–20}. However, as the composition of human islets varies dramatically both within and between individuals¹⁰, with alterations in the alpha-to-beta cell ratio in patients with T2D owing to reduced beta cell mass^{21,22} or possibly alpha cell expansion²³, it is essential to analyse T2D methylomes in a cell-type-specific manner. This is further underscored by the distinct global methylation patterns between alpha and beta cells^{24,25} and by the unique DNAm alterations observed in beta cells across the human lifespan and in T2D, as described below.

In this work, we leveraged the islet molecular phenotyping data generated by the Human Pancreas Analysis Program (HPAP; <https://hpap.pmacs.upenn.edu>)^{26,27}. To investigate epigenetic adaptation in beta cells across the human lifespan, we analysed genome-wide DNAm patterns in sorted beta and alpha cell populations from control (CTL) donors of various ages (here and throughout, ‘control’ refers to non-diabetic, autoantibody-negative individuals). This analysis revealed age-associated demethylation in beta cells, particularly in regulatory regions near islet transcription factor (TF) binding sites. Although these regions exist in a hypomethylated state in beta cells, the ongoing process of maintaining that state may require active demethylation, which counteracts maintenance methylation^{28,29}. This process may help maintain enhancer activity and sustain stable expression of key beta cell function genes to preserve cell identity throughout the long lifespan of beta cells. By contrast, alpha cells exhibited a subtler and opposite age-related trend, with a predominance of hypermethylation even in active regulatory regions.

Interestingly, we noted a beta cell-specific additional demethylation process in T2D compared to CTL, suggestive of an intensified compensatory response. By contrast, alpha cells from diabetic donors exhibited minimal methylation changes compared to healthy donors. Our findings suggest that in healthy individuals, the beta cell epigenome supports lifelong adaptation to metabolic demand. In T2D, however, enhanced demethylation probably reflects mounting stress on beta cells as diabetes progresses, representing an intensified attempt to maintain beta cell function that ultimately becomes unsustainable.

Results

DNA methylation patterns distinguish alpha and beta cell regulatory landscapes

DNAm has a crucial role in gene silencing, which is essential for maintaining cell type identity and cellular expression programmes throughout the lifespan and across cell divisions¹⁵. This stable methylation pattern is established by regulated processes of methylation and demethylation, and it is preserved by the activity of maintenance methyltransferase (DNMT1) as well as de novo methyltransferases such as DNMT3A^{30,31}. To confirm that our dataset captures robust cell

identity differences, quality control clustering of all 154 HPAP methylome samples shows clear separation between alpha, beta and exocrine cells regardless of sex, ancestry, age, diabetes status and assay type, with the outliers in each branch corresponding to samples with a low purity score (Extended Data Fig. 1).

To characterize the cell-type-specific methylation landscapes of pancreatic alpha and beta cells in our cohort, we compared methylomes from 14 CTL donors with high sample purity in both cell types (average (\pm s.d.) purity scores of $86 \pm 6\%$ and $91 \pm 7\%$ for alpha and beta cells, respectively; see Supplementary Table 1). The donors in this comparison represented an age range from 26 to 58 years. Principal component analysis (PCA) of methylation levels revealed that the cell identity of the sample accounted for 44% of the variance (Fig. 1a). Comparison of methylation profiles between alpha and beta cells identified 78,389 differentially methylated regions (DMRs) with a false discovery rate (FDR) of <0.01 and $|\Delta| > 10\%$ (Fig. 1b), whose distribution of average DNAm differences is shown in Fig. 1c.

We next focused on the 7,522 DMRs with the strongest effect sizes ($|\Delta| > 40\%$) and analysed the signals from published islet chromatin immunoprecipitation sequencing (ChIP-seq) and alpha and beta single-nucleus assay for transposase-accessible chromatin with sequencing (snATAC-seq) experiments across 10 kb regions centred at these DMRs (see Methods). This analysis revealed that regions hypomethylated in both beta and alpha cells were enriched for active chromatin marks and depleted of repressive marks (Fig. 1d). Consistently, hypomethylated regions in beta and alpha cells overlapped with open chromatin in each respective cell type (Fig. 1e). Finally, analysis of published TF binding data for whole islets³² revealed that binding sites for *FOXA2*, *MAFB* and *NKX2.2*, which are expressed in both alpha and beta cells, are mostly hypomethylated in both cell types, whereas binding sites for *NKX6.1* and *PDX1*, which are specific to beta cells, are predominantly hypomethylated in beta cells (Fig. 1e). These findings further demonstrate that alpha-cell-specific and beta-cell-specific hypomethylated regions are enriched in cell-type-specific regulatory elements, extending prior observations³³.

To test which gene sets are associated with hypomethylation in alpha and beta cells, we applied a hypergeometric test using DMRs selected with thresholds of FDR < 0.01 and $|\Delta| > 40\%$, considering genes annotated as DMR-distal, as described in Methods. This analysis showed that although common biological pathways important for both cell types, such as regulation of secretion and exocytosis, are associated with hypomethylation in both alpha and beta cells, other gene sets are specifically associated with hypomethylation in either cell type (Fig. 1f). For example, genes critical for beta cell function, such as *ADCYAPI*, *IAPP*, *INS*, *ABCC8* and *SYT7* (‘BETA_GENES’ in Fig. 1f and Supplementary Table 9), as well as beta-cell-specific TFs including *PDX1*, *NKX6.1*, *MNX1*, *PAX6* and *SIX3* (‘GO_ENDOCRINE_SYSTEM_DEVELOPMENT’ in Fig. 1f and Supplementary Table 9) are associated with hypomethylation in beta cells. By contrast, hypomethylation in alpha cells is associated with alpha cell function genes such as *GCG*, *DPP4*, *FAP*, *FEV* and *ADRBI* (Beta-1 Adrenergic Receptor), the latter known to stimulate glucagon secretion under adrenergic stress³⁴ (‘ALPHA_GENES’ in Fig. 1f and Supplementary Table 10).

Age-progressive DNA methylation loss in beta cell regulatory regions

Beta cells are long-lived cells that must continually adapt to fluctuating metabolic demands³⁵. These ongoing adaptations may be supported by the accumulation of epigenetic changes over time. Unlike gene expression, which is highly variable across individuals and becomes increasingly heterogeneous with age³⁶, DNAm provides a more stable epigenetic signature that reflects cellular identity and differentiation state. Although age-related DNAm changes have been documented in blood and brain tissues^{37,38}, they have not been studied in human beta cells. To address this knowledge gap, we analysed DNAm profiles from

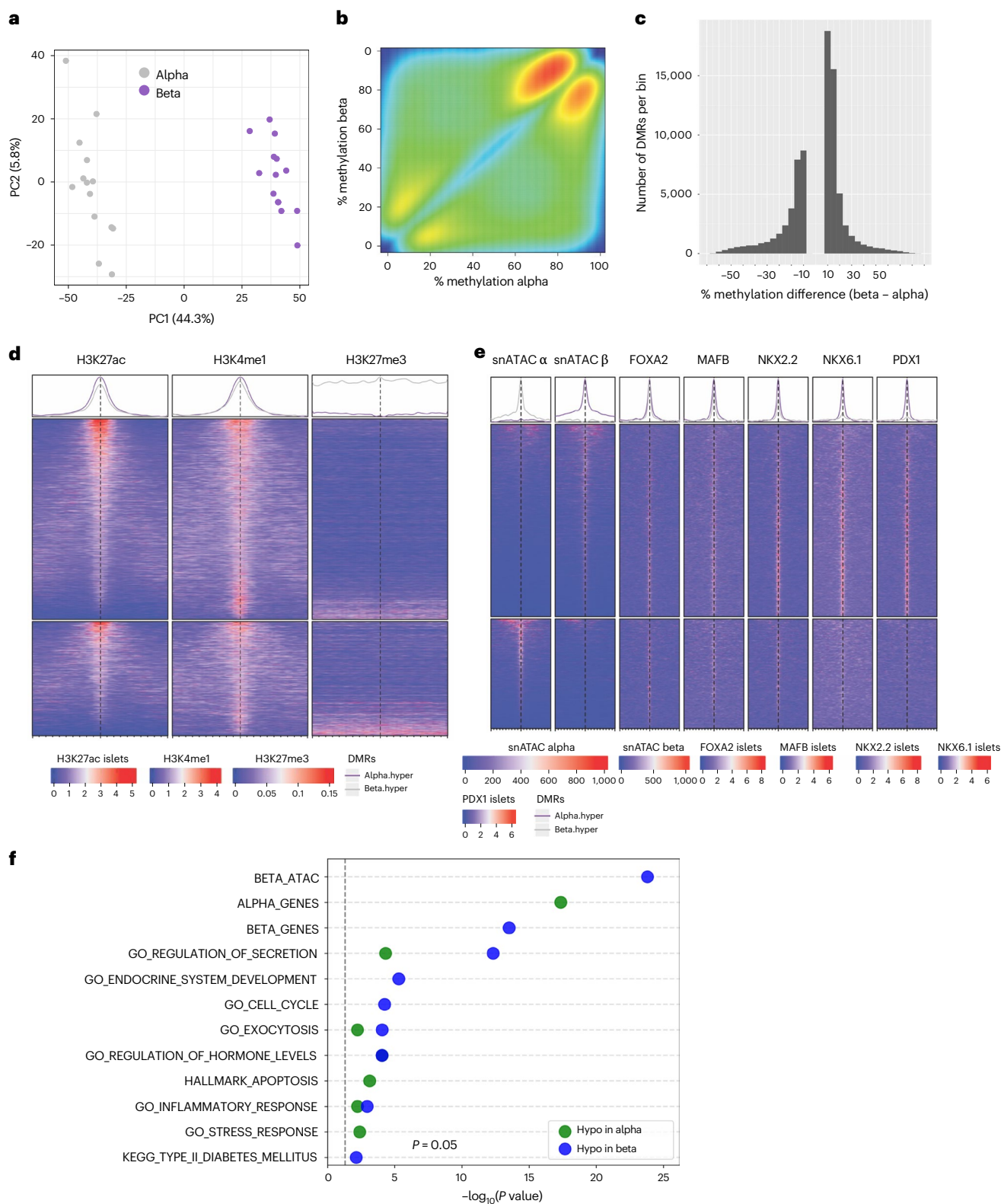


Fig. 1 | DNAm distinguishes alpha and beta cells in association with their cell-type-specific regulatory landscapes. **a**, Scatterplot of the first two principal components from PCA of DNAm CTL alpha and beta cells, showing separation by cell type along PC1. **b**, Methylation scatterplot. Smooth scatterplot of beta versus alpha cell methylation values (as %) in CTL donors for 78,389 DMRs with an FDR < 0.01 and $|\Delta| > 10\%$. **c**, Effect size distribution, showing the difference in average methylation between alpha and beta cells from the CTL donor DMRs shown in **b**. **d**, **e**, Enrichment heatmaps. Enrichment plot of signal intensity for

islet histone marks (ChIP-seq^{32,67}) (**d**) and chromatin accessibility (snATAC-Seq, HPAP) and TF binding sites (whole islet, ChIP-seq³²) (**e**) across top alpha-beta DMRs (FDR < 0.01, $|\Delta| > 40\%$). Each row shows the signal over the 10 kb region centred at one of 7,522 DMRs. Top, regions hypomethylated in beta cells; bottom, regions hypomethylated in alpha cells. **f**, Gene set enrichment results for hypomethylated DMRs in alpha (green) and beta (blue) cells, based on DMR-distal genes (FDR < 0.01, $|\Delta| > 40\%$, CTL alpha vs beta). The x-axis displays $-\log_{10}$ of the unadjusted P values from a one-sided hypergeometric test.

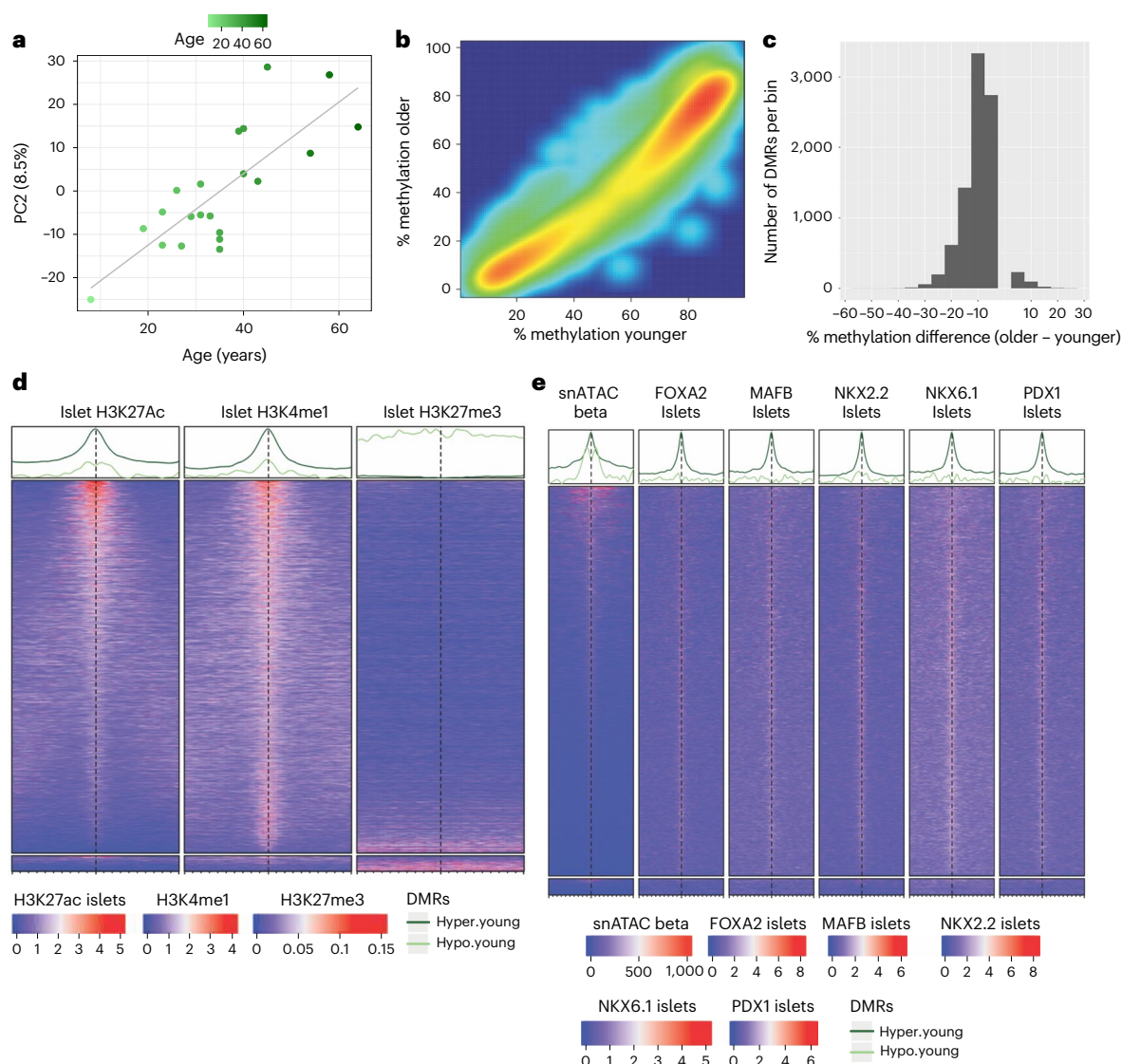


Fig. 2 | Progressive loss of DNAm at regulatory regions in beta cells with age (part I). **a**, PCA of DNAm in CTL beta cells. Scatterplot of PC2 versus age, illustrating a strong correlation ($R^2 = 0.62$, two-sided Pearson correlation $P = 2.3 \times 10^{-5}$) between the two variables. **b**, Methylation scatterplot. Smooth scatterplot of beta cell methylation values (as %) in older (39–58 years old) versus younger (18–35 years old) CTL donors across 8,748 age-associated DMRs ($FDR < 0.01$ and $|\Delta| > 5\%$), illustrating age-related demethylation. **c**, Effect size distribution. Distribution of average methylation differences between older and

younger donors for the DMRs shown in **b**. **x** axis, % difference (older – younger); **y** axis, number of DMRs per bin. **d,e**, Enrichment heatmaps. Enrichment plot of signals from islet histone marks (**d**) and chromatin accessibility (snATAC-Seq, beta cells) and TF binding (ChIP-seq, whole islets) (**e**) across 8,748 age-associated DMRs ($FDR < 0.01$ and $|\Delta| > 5\%$) in beta cells from CTL donors. Each row shows the signal over the 10 kb region centred at one DMR. Top, regions hypomethylated in older donors; bottom, hypomethylated in younger donors.

pancreatic beta cells collected from 21 HPAP CTL donors across a broad age spectrum from 8 to 64 years old. UXM-estimated purity scores had a mean (\pm s.d.) of $91 \pm 6\%$. Moreover, based on the UXM-estimated cell type composition (see Methods), there was no strong association between age and the proportion of cells of any given type (maximum $R^2 = 0.1$), including monocytes and macrophages ($R^2 = 0.048$). Supplementary Table 2 provides the characteristics of the samples used in this comparison. PCA of methylation levels indicated that PC2 was significantly correlated with age ($R^2 = 0.62$, $P < 0.001$) (Fig. 2a). In this comparison we analysed age as a numeric covariate, and to measure effect size, we defined Δ as the difference in average methylation between the group of older donors aged 39–58 years and that of younger donors aged 18–35 years (see Methods). This comparison identified 8,748 DMRs at the thresholds of $FDR < 0.01$, $|\Delta| > 5\%$, with a striking 96% (8,394 DMRs) showing hypomethylation with age (Fig. 2b). Although the magnitude of methylation changes was generally

modest, with most DMRs showing $|\Delta| < 30\%$ (Fig. 2c), the differences were consistent and statistically significant. Therefore, despite the small effect size, ageing in beta cells is associated with a robust and widespread hypomethylation signature.

Next, we analysed the signals from islet ChIP-seq and beta snATAC-seq experiments across 10 kb regions centred at these age-related beta cell DMRs (see Methods) (Fig. 2d,e). Our analysis revealed that regions hypomethylated with age are predominantly located in beta-cell-specific active regulatory chromatin domains, as evidenced by significant enrichment for H3K27ac, H3K4me1, beta-ATAC regions and binding sites for islet and beta-cell-specific TFs such as *NKX6.1* and *PDX1*. To validate these findings, we assessed the average methylation levels within previously identified islet active enhancer regions³², which revealed subtle progressive demethylation with age (Fig. 3a). The distribution of slopes from linear fits of methylation versus age in these enhancer regions, representing the rate of change

of DNAm per year, is clearly shifted towards negative values (Fig. 3b). Although the absolute values of the slopes are modest, they reflect a consistent directional trend, with 82% of the 28,813 fits exhibiting negative slopes and relatively strong negative associations, as indicated by the corresponding Pearson correlation coefficients (median Pearson correlation coefficient = -0.35 ; Fig. 3c) and P values (median $P = 0.06$; Fig. 3d). Notably, enhancer regions can be actively demethylated by TET enzymes, which also help to protect against age-related functional decline in other tissues such as the brain^{28,39}.

To explore the mechanisms driving age-associated demethylation in active enhancers, we examined methylation levels at TF binding sites of *NKX6.1* and *PDX1*, which are enriched in beta cell enhancers⁴⁰, focusing on those showing the greatest variation across age. We observed progressive demethylation with increasing donor age at these sites (Fig. 3e,i), and the distribution of slopes from linear fits of methylation versus age was clearly shifted toward negative values, shown for *PDX1* in Fig. 3f and for *NKX6.1* in Fig. 3j. For regions with negative slopes, the median Pearson correlation was -0.56 with a median P value of 0.004 for *PDX1* (Fig. 3g,h), and -0.55 with a median P value of 0.005 for *NKX6.1* (Fig. 3k,l).

We next asked whether age-related DMRs in beta cells were enriched near genes associated with specific biological pathways or gene sets. Using DMRs filtered by $FDR < 0.01$ and $|\Delta| > 10\%$ and considering DMR-distal genes (as defined in Methods), we found that hypomethylated regions in older donors were enriched in beta-cell-specific regulatory regions, such as beta cell ATAC peaks, and near genes involved in beta cell function, cell cycle regulation and, notably, DNA damage response (DDR) and T2D-associated genes, whereas the disallowed gene set showed no enrichment (Fig. 3m and Supplementary Table 11). To explore potential links to beta cell heterogeneity, we assessed enrichment for subtype gene signatures^{41,42} and found that genes characteristic of the ST8SIA1-positive and β HI subpopulations were enriched among beta cell age-related hypomethylated DMRs (Fig. 3m and Supplementary Table 11). However, this enrichment could be influenced by age-related changes in the proportion of these subpopulations, as our methylomes represent a bulk signal integrating inputs from diverse beta cell populations. Gene set enrichment analysis (GSEA) of HPAP single-cell RNA sequencing (scRNA-seq) data from donors in a similar age range revealed upregulation of the p53 pathway in older individuals, including increased expression of *CDKN2A*, *CDKN1A* and *CDKN2B* (Extended Data Fig. 2a and Supplementary Table 12), supporting progressive activation of stress response and senescence programmes in beta cells with age. In line with previous reports¹⁴, GSEA also showed age-associated downregulation of the HALLMARK beta cell gene set as a whole (Extended Data Fig. 2b and Supplementary Table 13), although most individual genes were not significantly downregulated (Extended Data Fig. 2c). The mild

downregulation of this gene set is unlikely to compromise beta cell identity or function, as key functional pathways such as hormone secretion and oxidative phosphorylation remain unchanged with age, along with the expression of major beta cell identity genes such as *PDX1* and *NEUROD1* (Extended Data Fig. 2c).

To further explore whether the observed demethylation with age was directly correlated with adaptation, we analysed the same 21 beta cell methylomes for correlation with body mass index (BMI) and with GSIS (measured by the ratio of glucose-stimulated [B] versus basal [A] insulin secretion; for details see Methods). The R^2 for BMI versus age in this dataset was 0.18. The correlations between the first five beta cell methylation-based PCs and BMI were much weaker (R^2 ranging from 0.009 to 0.21) than the noted strong correlation between PC2 and age ($R^2 = 0.62$). A BMI-based DMR analysis with the same thresholds as those used for age identified 599 regions, and only 47 of the 8,394 age-demethylated DMRs were among these. As for GSIS, the R^2 for the B/A ratio versus age was negligible (0.0018). The correlations between the first five beta cell methylation-based PCs and the B/A ratio were much weaker (R^2 ranging from 0 to 0.18) than the noted strong correlation between PC2 and age. A GSIS-based DMR analysis with the same thresholds as those used for age identified only 20 regions, none of which were among the 8,394 age-demethylated DMRs. These observations, together with heatmaps of the age-hypomethylated regions in healthy beta cells ordered by age, BMI and GSIS (Extended Data Fig. 3), indicate that BMI and GSIS are not the main drivers of the age-demethylated DMRs identified above.

In contrast to beta cells, alpha cells show progressive DNA hypermethylation with age

For alpha cells, we analysed 14 samples from CTL donors spanning an age range from 18 to 58 years. UXM-estimated purity scores had a mean (\pm s.d.) of $87 \pm 5\%$. Based on the UXM-estimated cell type composition (see Methods), there was no association between age and the proportion of cells of any given type (maximum $R^2 = 0.22$), including monocytes and macrophages ($R^2 = 0.074$). Supplementary Table 3 provides the characteristics of the samples used in this comparison. PCA of methylation levels indicated that PC2 was significantly correlated with age ($R^2 = 0.77$, $P < 0.001$) (Fig. 4a). We analysed the CTL alpha cell age comparison in the same manner as described above for beta cells using the same thresholds of $FDR < 0.01$ and $|\Delta| > 5\%$ and identified 1,466 DMRs, of which, surprisingly, 1,344 (92%) were hypermethylated with age, although the magnitude of methylation changes was modest, with most DMRs showing $|\Delta| < 20\%$ (Fig. 4b–c). A subset of age-dependent hypermethylation occurred in active regulatory domains, but a higher proportion occurred in repressed regions that are not bound by TFs, as illustrated by the enrichment heatmaps of signals from the islet CHIP-seq and alpha snATAC-seq experiments

Fig. 3 | Progressive loss of DNAm at regulatory regions in beta cells with age (part II). a, Enhancer methylation heatmap. Heatmap of average beta cell methylation at islet active enhancer regions³² (rows) across 21 HPAP CTL donors (columns), ordered by age, illustrating progressive demethylation with age. Methylation values are shown as fractions between 0 and 1. b, Linear fit slopes for enhancers. Violin plot of the slopes of linear fits to methylation versus age, corresponding to the regions in a. Mean slope = -0.0012 ; median slope = -0.0008 . c, d, Pearson correlations for enhancers. Boxplot of Pearson correlation coefficients (c) and corresponding P values (d) for the 23,705 regions with negative methylation–age slopes from a. Boxplot parameters: middle line, median; box upper (resp. lower) bound, 3rd (resp. 1st) quartile; upper/lower whisker extends to the largest/smallest value within $1.5 \times$ the interquartile range (IQR); individual points, outliers. e, *PDX1* binding sites methylation heatmaps. Heatmap of average beta cell methylation at *PDX1* binding sites³², showing the 500 peaks with the greatest variability across CTL donors, ordered by age. Note the demethylation trend with age. f, Linear fit slopes for *PDX1* binding sites. Violin plot of the slopes of linear fits to methylation versus age, corresponding to the regions in e. g, h, Pearson correlations for *PDX1* binding sites. Boxplot of Pearson

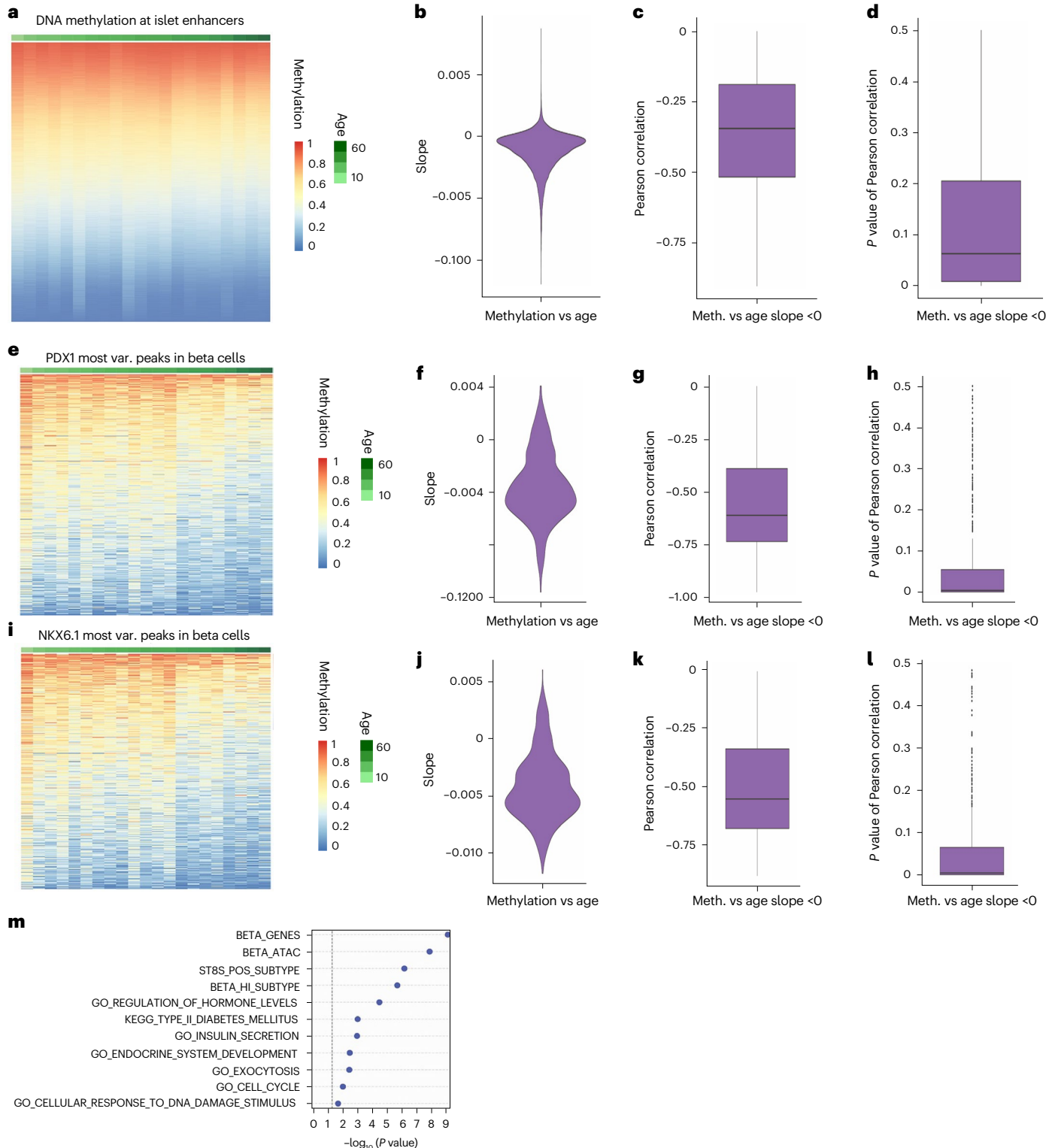
correlation coefficients (g) and corresponding P values (h) for the 447 regions with negative methylation–age slopes from e. Boxplot parameters: middle line, median; box upper (resp. lower) bound, 3rd (resp. 1st) quartile; upper/lower whisker extends to the largest/smallest value within $1.5 \times$ IQR; individual points, outliers. i, *NKX6.1* binding sites methylation heatmaps. Heatmap of average beta cell methylation at *NKX6.1* binding sites³², showing the 500 peaks with the greatest variability across CTL donors, ordered by age. Note the demethylation trend with age. j, Linear fit slopes for *NKX6.1* binding sites. Violin plot of the slopes of linear fits to methylation versus age, corresponding to the regions in i. k, l, Pearson correlations for *NKX6.1* binding sites. Boxplot of Pearson correlation coefficients (k) and corresponding P values (l) for the 448 regions with negative methylation versus age slopes from i. Boxplot parameters: middle line, median; box upper (resp. lower) bound, 3rd (resp. 1st) quartile; upper/lower whisker extends to the largest/smallest value within $1.5 \times$ IQR; individual points, outliers. m, Gene set enrichment results. Gene set enrichment for hypomethylated DMRs in beta cells, based on DMR-distal genes ($FDR < 0.01$ and $|\Delta| > 10\%$) from the CTL beta age comparison. The x axis displays $-\log_{10}$ of the unadjusted P values from a one-sided hypergeometric test.

correlation coefficients (g) and corresponding P values (h) for the 447 regions with negative methylation–age slopes from e. Boxplot parameters: middle line, median; box upper (resp. lower) bound, 3rd (resp. 1st) quartile; upper/lower whisker extends to the largest/smallest value within $1.5 \times$ IQR; individual points, outliers. i, *NKX6.1* binding sites methylation heatmaps. Heatmap of average beta cell methylation at *NKX6.1* binding sites³², showing the 500 peaks with the greatest variability across CTL donors, ordered by age. Note the demethylation trend with age. j, Linear fit slopes for *NKX6.1* binding sites. Violin plot of the slopes of linear fits to methylation versus age, corresponding to the regions in i. k, l, Pearson correlations for *NKX6.1* binding sites. Boxplot of Pearson correlation coefficients (k) and corresponding P values (l) for the 448 regions with negative methylation versus age slopes from i. Boxplot parameters: middle line, median; box upper (resp. lower) bound, 3rd (resp. 1st) quartile; upper/lower whisker extends to the largest/smallest value within $1.5 \times$ IQR; individual points, outliers. m, Gene set enrichment results. Gene set enrichment for hypomethylated DMRs in beta cells, based on DMR-distal genes ($FDR < 0.01$ and $|\Delta| > 10\%$) from the CTL beta age comparison. The x axis displays $-\log_{10}$ of the unadjusted P values from a one-sided hypergeometric test.

over the 10 kb regions centred at these DMRs (Extended Data Fig. 4; see Methods for details).

We next examined whether age-related DMRs in alpha cells were enriched near specific pathways or gene sets. Using an FDR < 0.01 and $|\Delta| > 10\%$ cutoff, we did not detect enrichment for specific pathways or gene sets in association with either hypomethylated or hypermethylated regions with age in alpha cells. Analysis of pseudo-bulk alpha cell gene expression data across age did not reveal a correlation with gene silencing or reduced expression with age, possibly because of the low effect size and the higher degree of variability of transcriptomic versus CpG methylation data.

To further explore the discrepancy between alpha and beta cells, we compared their methylation levels across ages at binding sites for *FOXA2* and *NKX2.2*, two TFs expressed at similar levels in both cell types^{32,43–46}. We used the same number of available samples (13) for each cell type (mostly common donors and, when not available, aged-matched donors) and, for each cell type separately, considered the 500 binding sites whose methylation varied most across ages; that is, focusing on sites most affected by age in that cell type. As illustrated in Fig. 4d,e and Extended Data Fig. 5, we observed subtle progressing demethylation of these regions with age in beta cells, whereas the trend in alpha cells was opposite. The distribution of slopes from linear fits



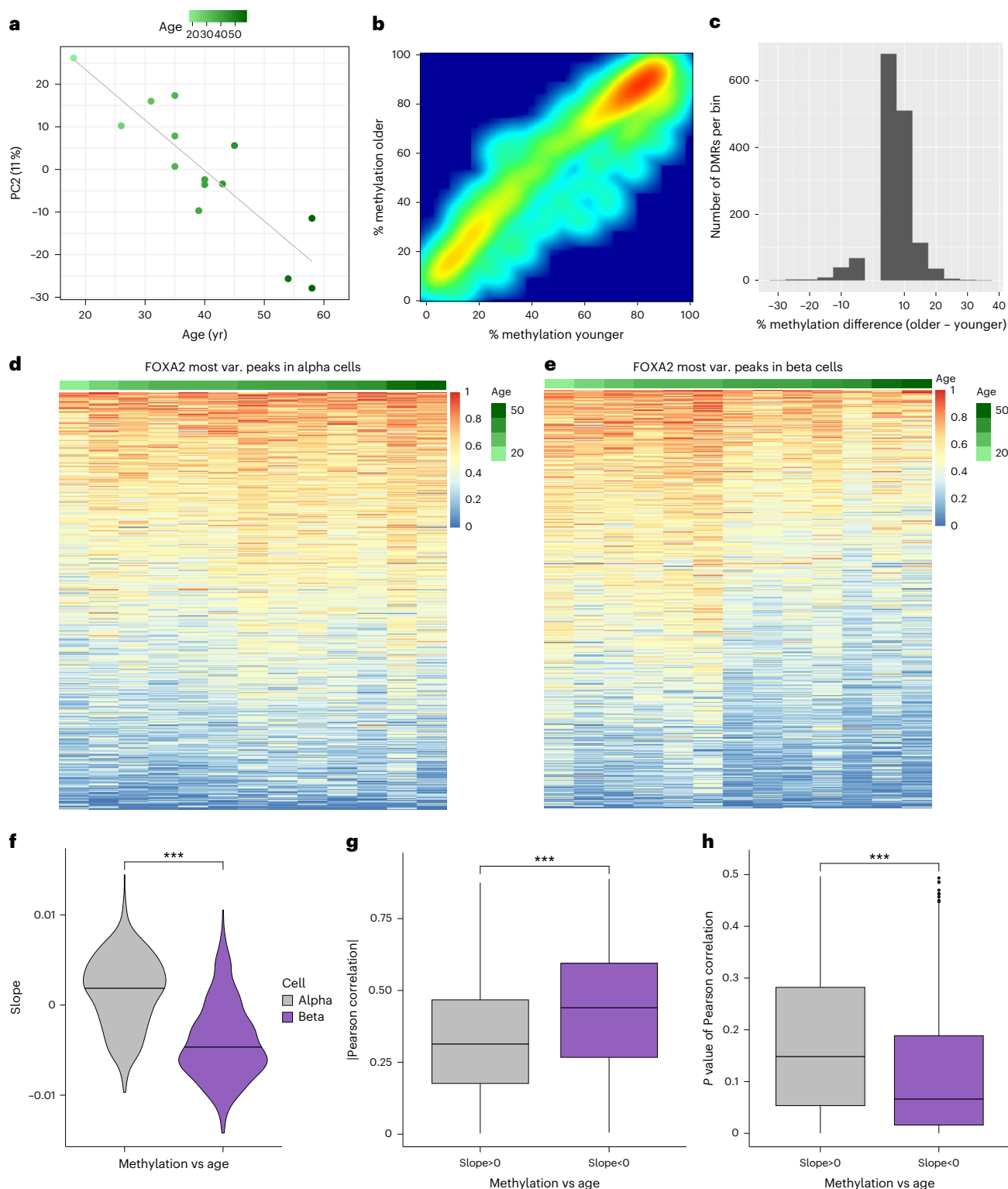


Fig. 4 | Alpha cells show modest age-related DNA hypermethylation, opposite to the trend in beta cells. **a**, PCA of DNAm in CTL alpha cells. Scatterplot of PC2 versus age, showing a strong correlation ($R^2 = 0.77$, two-sided Pearson correlation $P = 3.8 \times 10^{-5}$). **b**, Methylation scatterplot. Smooth scatterplot of alpha cell methylation (%) in older (39–58 years old) versus younger (18–35 years old) CTL donors across 1,466 age-associated DMRs (FDR < 0.01, $|\Delta| > 5\%$), illustrating subtle hypermethylation in older donors. **c**, Effect size distribution. Distribution of average methylation differences (older – younger) for the DMRs shown in **b**. x axis, % difference (older – younger); y axis, number of DMRs per bin. **d, e**, FOXA2 binding sites methylation heatmaps. Heatmaps of average CpG methylation at FOXA2 binding sites³² in alpha (**d**) and beta (**e**) cells. Shown are the 500 most

variable peaks (per cell type) across 13 age-matched donors. **f**, Linear fit slopes for FOXA2 binding sites. Violin plots of slopes from linear fits of methylation versus age at the regions shown in **d** and **e**, for alpha and beta cells. Asterisks indicate a two-sided Wilcoxon $P < 0.001$ (in this case, $P < 2.22 \times 10^{-16}$). **g, h**, Pearson correlations for FOXA2 binding sites. Boxplots of absolute Pearson correlation coefficients (**g**) and correlation P values (**h**) for methylation versus age at the 332 regions with slope >0 in alpha cells and the 410 regions with slope <0 in beta cells from **f**. Boxplot parameters: middle line, median; box upper (resp. lower) bound, 3rd (resp. 1st) quartile; upper/lower whisker extends to the largest/smallest value within 1.5 × IQR; individual points, outliers. Asterisks indicate a two-sided Wilcoxon $P < 0.001$ ($P = 7.1 \times 10^{-10}$ in both cases).

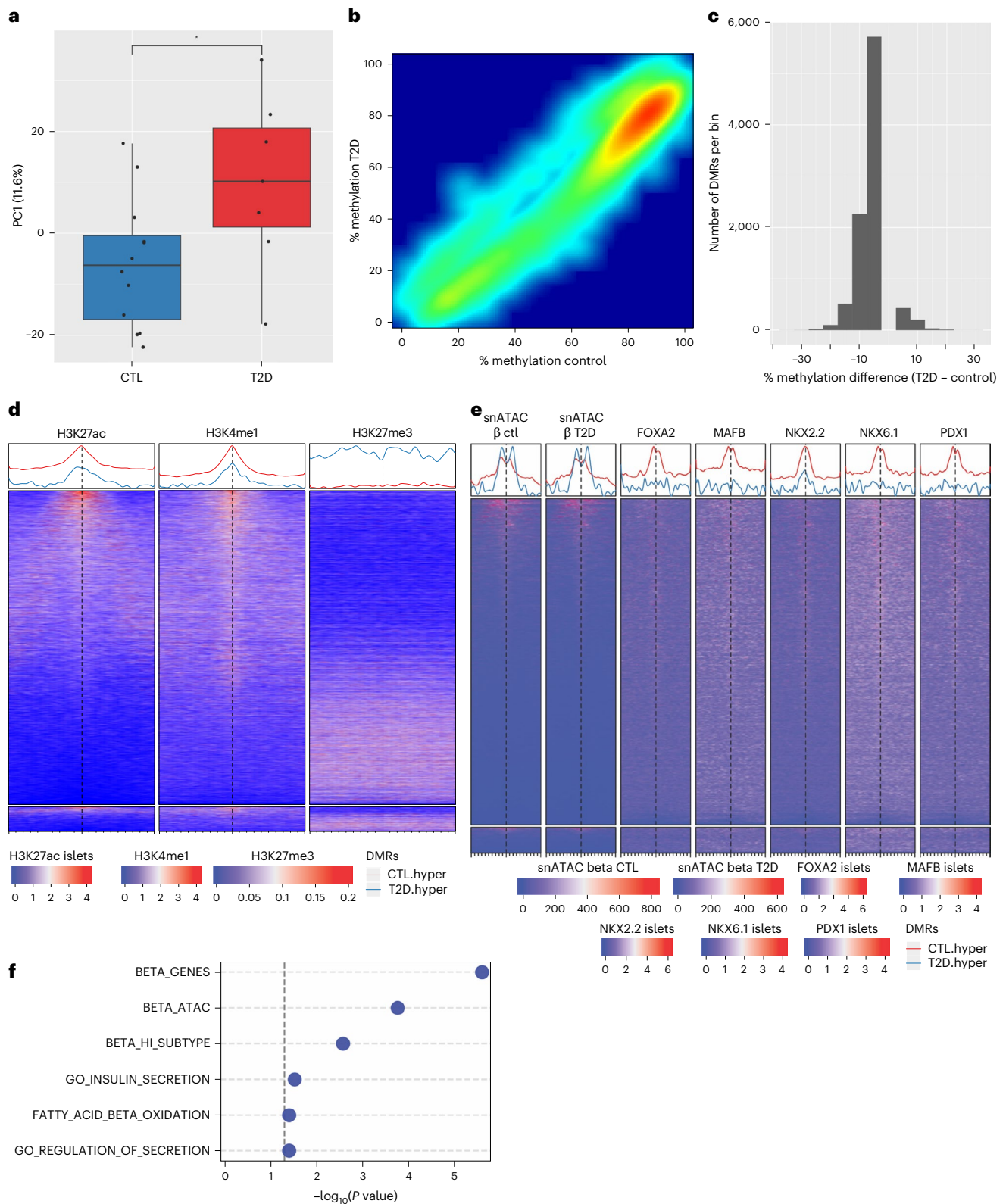


Fig. 5 | Beta cells exhibit accelerated DNA demethylation in T2D (part I). **a**, PCA of DNAm in beta cells from CTL and T2D donors. Boxplots of the PC1 stratified by condition for 12 CTL and seven T2D donors. Boxplot parameters: middle line, median; box upper (resp. lower) bound, 3rd (resp. 1st) quartile; upper/lower whisker extends to the largest/smallest value within 1.5× IQR; each donor is represented by a point. Asterisk indicates a two-sided Wilcoxon $P < 0.05$ ($P = 0.03$ in this case). **b**, Methylation scatterplot. Smooth scatterplot of beta cell methylation (%) in T2D versus CTL donors across 9,296 DMRs ($FDR < 0.05$, $|\Delta| > 5\%$), illustrating subtle hypomethylation in T2D. **c**, Effect size distribution. Distribution of average methylation differences (T2D - CTL)

for the DMRs shown in **b**. x axis, % difference (T2D - CTL); y axis, number of DMRs per bin. **d, e**, Enrichment heatmaps. Enrichment plot of signals from islet histone marks (**d**) and chromatin accessibility (snATAC-Seq, beta cells) and TF binding (ChIP-seq, whole islets) (**e**) across 9,296 DMRs ($FDR < 0.05$, $|\Delta| > 5\%$) from the T2D versus CTL beta cell comparison. Each row shows the signal over the 10 kb region centred at one DMR. Top, regions hypomethylated in T2D; bottom, hypomethylated in CTL beta cells. **f**, Gene set enrichment results. Gene set enrichment for hypomethylated DMRs based on DMR-distal genes ($FDR < 0.05$, $|\Delta| > 10\%$) from the T2D versus CTL beta cell comparison. The x axis displays $-\log_{10}$ of the unadjusted P values from a one-sided hypergeometric test.

of methylation versus age in these regions is shifted towards positive values in alpha cells and negative values in beta cells, with the shift more evident at *FOXA2* binding sites than at *NKX2.2* binding sites in alpha cells (Fig. 4f and Extended Data Fig. 6a). Moreover, the regions with negative slopes in beta cells correspond to significantly better linear fits than the regions with positive slopes in alpha cells (Fig. 4g,h and Extended Data Fig. 6b,c).

Together, these findings demonstrate that despite being closely related cell types residing within the same functional unit, beta and alpha cells undergo opposing age-related DNA methylation trajectories. Beta cells exhibit progressive hypomethylation at regulatory regions, particularly at TF binding sites, potentially reflecting their adaptive, metabolically responsive nature, whereas alpha cells do not show this demethylation process but instead display gradual hypermethylation, predominantly in non-active chromatin regions.

T2D is associated with premature hypomethylation in beta cells

A recent study using medium-throughput DNAm and RNA-seq analysis of whole human islets reported DNAm changes associated with impaired insulin secretion and reduced expression of beta-cell-related genes in T2D donors²⁰. However, given that islet cell composition varies between individuals¹⁰, and T2D islets often exhibit altered alpha-to-beta cell ratios owing to beta cell loss^{21,22} or possibly alpha cell expansion²³, whole-islet analysis can obscure cell-type-specific epigenetic signals. This is especially relevant given the marked differences in DNAm profiles between alpha and beta cells and the opposing age-related methylation changes between the two cell types reported above. To capture beta-cell-specific changes in T2D, we analysed beta cell samples from 12 CTL and seven donors with T2D, with similar ages ranging from 33 to 64 years. All samples had high UXM-estimated purity, with a mean (\pm s.d.) of $91 \pm 7\%$ for CTL and $89 \pm 4\%$ for T2D donors (see Supplementary Table 4 for characteristics). PCA of methylation levels revealed an association between PC1 and disease status (two-sided Wilcoxon $P = 0.04$; Fig. 5a).

Using FDR < 0.05 and $|\Delta| > 5\%$ thresholds, we identified 9,296 DMRs, the majority of which (8,619; 93%) were hypomethylated in T2D, with most showing modest differences ($|\Delta| < 20\%$) (Fig. 5b,c). About half of the hypomethylated regions in T2D were enriched for H3K4me1, marking primed enhancers, while a subset also carried H3K27ac, suggesting an active regulatory state. The remaining hypomethylated regions were enriched for the repressive mark H3K27me3 (Fig. 5d). Some hypomethylated regions also showed enrichment for TF binding sites, particularly those bound by *FOXA2*, *NKX2.2* and *PDX1* (Fig. 5e).

We then examined DMR-distal genes to DMRs with FDR < 0.05 and $|\Delta| > 10\%$ and found enrichment in T2D-associated demethylation for genes involved in beta-cell-related pathways, mirroring the pattern observed in age-associated hypomethylation (Fig. 5f and Supplementary Table 14). In addition, these regions were enriched for the β HI beta cell subpopulation gene set^{41,42}, whose relative proportion increases in T2D, suggesting that this enrichment may partly reflect over-representation of this subtype. Notably, T2D hypomethylated DMRs showed no enrichment near disallowed genes⁴⁷ (Fig. 5f and Supplementary Tables 8 and 14), which were also not upregulated in our dataset. By contrast, no significant pathway enrichment was observed for hypermethylated regions, consistent with a less specific, stochastic process. To assess the potential functional consequences of these methylation changes, we examined gene expression in beta cells from CTL ($n = 13$) and T2D ($n = 15$) donors of similar age using HPAP scRNA-seq data and found that T2D-associated hypomethylated DMRs did not show a direct correlation with upregulation of their associated genes. In fact, only 1.6% (about 20 genes) of the 1,212 genes associated with hypomethylated DMRs in T2D were differentially expressed (mostly upregulated), and none are known beta cell identity or function genes,

suggesting a limited direct role of T2D-associated demethylation in regulating gene expression levels. Analysis of additional scRNA-seq datasets comparing T2D and CTL beta cells^{48,49} likewise showed no enrichment of genes upregulated in T2D near hypomethylated DMRs. However, although core beta cell identity genes such as *PDX1*, *NKX6.1*, *MAFA*, *ABCC8* and *KCNJ11* maintain stable expression levels in T2D donors (Extended Data Fig. 7a), we observed reduced expression of broader functional pathways, including oxidative phosphorylation, glycolysis and protein secretion (Supplementary Table 15 and Extended Data Fig. 7b). Genes from these pathways, which are largely not linked to hypomethylation, do not maintain stable expression (Extended Data Fig. 7c), supporting intact core identity program but compromised beta cell function in T2D.

Next, we compared average beta cell methylation levels at *PDX1* binding sites using seven CTL and seven T2D donors matched for age, selecting the 500 most variable sites across age within each condition. This analysis revealed that although demethylation at these sites tends to progress with age in CTL donors (Fig. 6a), as was shown above using a larger number of samples (Fig. 3e), this trend is less evident in beta cells from donors with T2D (Fig. 6b). The distribution of slopes from linear fits of methylation versus age at these regions was significantly more negative in CTL donors than those with T2D (Fig. 6c). The Pearson correlation coefficients for regions with negative slopes were also significantly more negative in CTL donors (Fig. 6d), and their associated P values trended lower (Fig. 6e). Although this analysis is based on a relatively small number of age-matched donors and should be interpreted with caution, the consistent differences in slope direction and correlation values across matched CTL and T2D samples support a more robust age-related demethylation process in non-diabetic donors at these regions. The lack of a clear age-related demethylation trajectory in T2D donors probably reflects already reduced methylation levels in beta cells early in life, possibly driven by chronic stress during diabetes progression. To illustrate this observation, we plotted the median methylation levels of the same *PDX1* binding sites in T2D and CTL donors matched for age. As shown in Fig. 6f, focusing on the peaks in the fifth quintile of the median methylation levels (-55 – 65%), T2D donors consistently exhibit lower methylation than age-matched controls across the age range. This pattern supports the idea that demethylation at these sites occurs earlier in life in T2D beta cells. Similar trends were observed at *FOXA2* and *NKX2.2* binding sites in the fifth quintile (Extended Data Fig. 8), further supporting this observation. We explored the possibility of a genetic link by examining the T2D-associated single nucleotide polymorphisms (SNPs) identified in previous work⁵⁰. GREGOR enrichment analysis did not detect a particularly significant enrichment of these SNPs and their proxies in the beta cell hypomethylated DMRs in T2D from our results ($P = 0.11$).

Finally, we performed an analysis of DNAm changes in alpha cells from nine T2D and 13 control donors matched for age (33–63 years) and with high UXM-estimated purity (mean \pm s.d., $87 \pm 5\%$ for CTL; $86 \pm 8\%$ for T2D; Supplementary Table 5). Despite the larger number of alpha cell samples compared to the beta cell analysis, we identified significantly fewer DMRs (1,574) between T2D and CTL alpha cells using the same thresholds (FDR < 0.05 and $|\Delta| > 5\%$) (Fig. 7a) and comparable to the numbers of DMRs in shuffled data (Supplementary Table 16). These DMRs showed a roughly equal distribution of hypomethylation and hypermethylation (Fig. 7b). Most were marked by the repressive histone modification H3K27me3 (Fig. 7c), while hypermethylated regions in T2D were also somewhat enriched for *NKX2.2* binding (Fig. 7d). Neither hypomethylated nor hypermethylated regions were associated with specific biological pathways.

Altogether, our data demonstrate that beta cells in T2D exhibit an accelerated demethylation pattern resembling age-related changes, predominantly in TF binding sites, a phenomenon not observed in alpha cells, and whose functional consequences remain to be investigated.

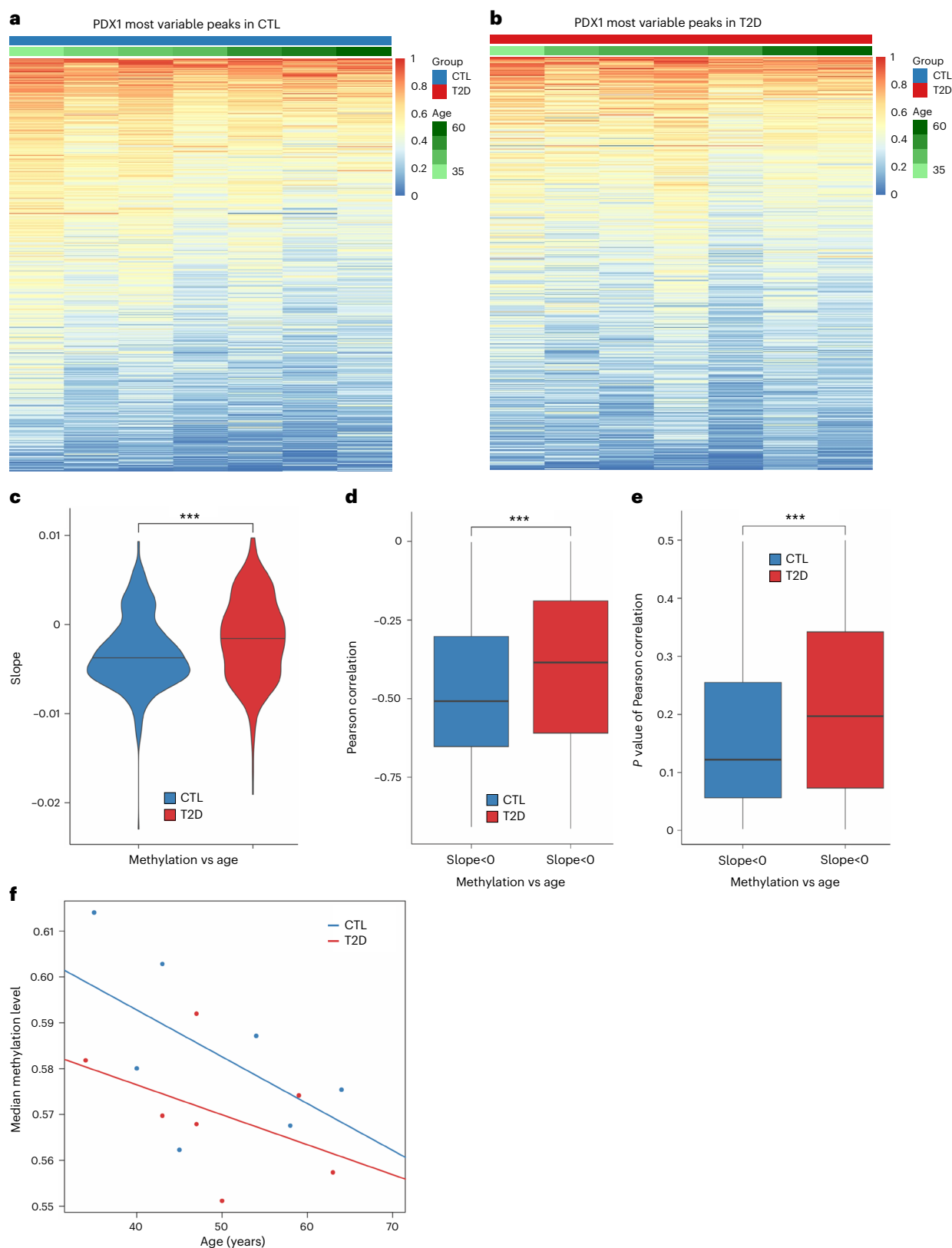


Fig. 6 | Beta cells exhibit accelerated DNA demethylation in T2D (part II). **a, b**, *PDX1* binding sites methylation heatmaps. Heatmaps of average beta cell methylation at *PDX1* binding sites³² in CTL (**a**) and T2D (**b**) donors. Shown are the 500 most variable peaks (separately, for CTL and T2D) across seven age-matched donors. **c**, Linear fit slopes for *PDX1* binding sites. Violin plots of slopes from linear fits of methylation versus age at the regions shown in **a** and **b**, for beta cells from CTL and T2D donors. Asterisks indicate a two-sided Wilcoxon $P < 0.001$ (in this case, $P = 2.8 \times 10^{-5}$). **d, e**, Pearson correlations for *PDX1* binding sites. Boxplots of Pearson correlation

coefficients (**d**) and corresponding P values (**e**) for methylation versus age at regions (398 for CTL and 310 for T2D) with slope of < 0 from **a** and **b**. Boxplot parameters: middle line, median; box upper (resp. lower) bound, 3rd (resp. 1st) quartile; upper/lower whisker extends to the largest/smallest value within $1.5 \times$ IQR; individual points, outliers. Asterisks indicate a two-sided Wilcoxon $P < 0.001$ ($P = 6.5 \times 10^{-5}$ in both cases). **f**, Methylation versus age in *PDX1* binding sites. Median methylation values across the *PDX1* binding sites in the fifth quintile of the median methylation levels for seven CTL (blue) and seven T2D (red) age-matched donors.

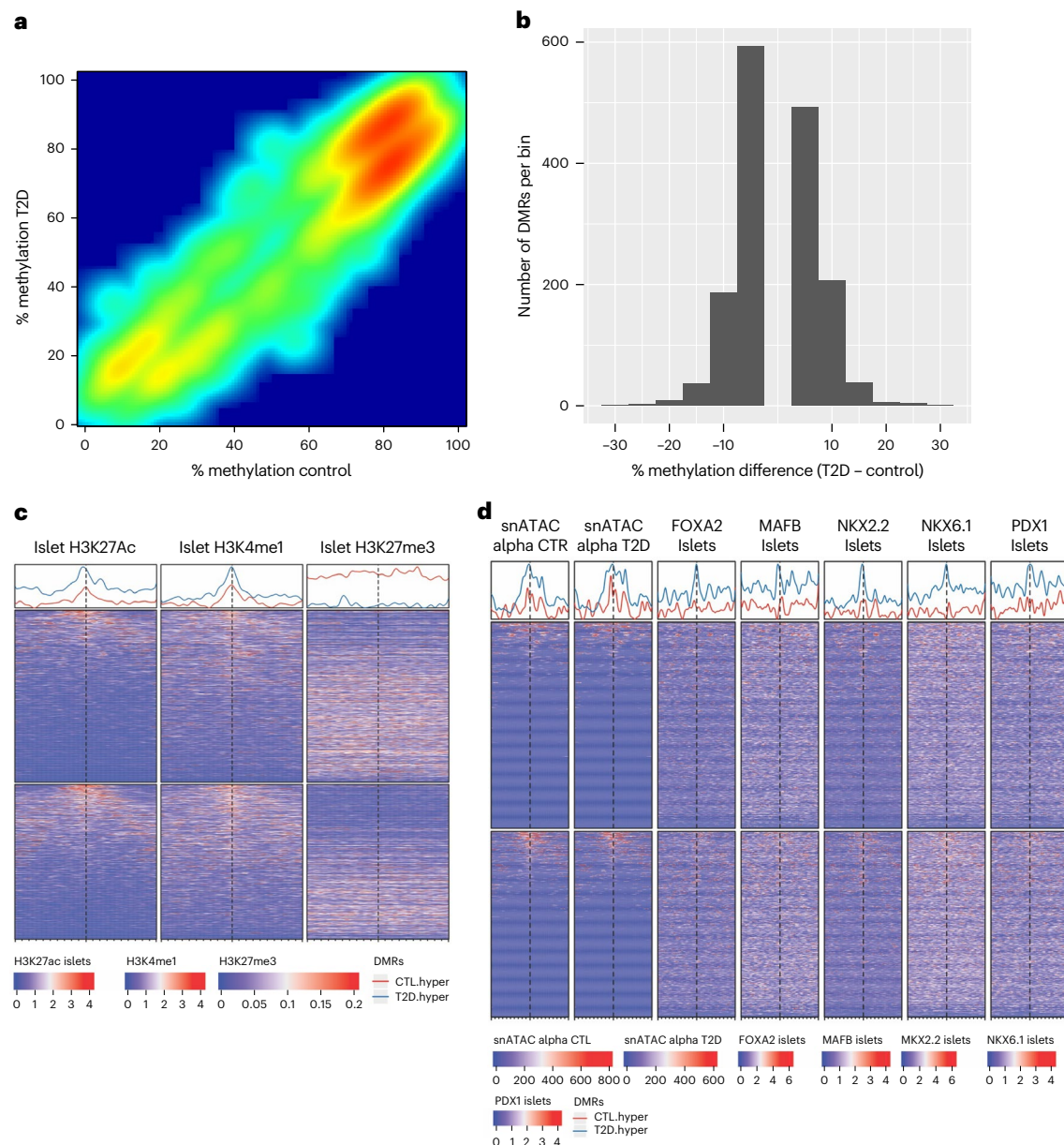


Fig. 7 | Alpha cells show minimal DNA methylation differences in T2D.

a, Methylation scatterplot. Smooth scatterplot of alpha cell methylation (%) in T2D versus CTL donors across 1,574 DMRs ($FDR < 0.05$, $|\Delta| > 5\%$), illustrating subtle, bidirectional methylation changes in T2D. **b**, Effect size distribution. Distribution of average methylation differences (T2D - CTL) for the DMRs shown in **a**. *x* axis: % difference (T2D - CTL); *y* axis, number of DMRs per bin.

c,d, Enrichment heatmaps. Enrichment plots of signals from islet histone marks (**c**) and chromatin accessibility (snATAC-seq, alpha cells) and TF binding (ChIP-seq, whole islets) (**d**) across 1,574 DMRs ($FDR < 0.05$, $|\Delta| > 5\%$) from the T2D versus CTL alpha cell comparison. Each row shows the signal over the 10 kb region centred at one DMR. Top, regions hypomethylated in T2D; bottom, hypomethylated in CTL alpha cells.

Discussion

This study leverages comprehensive human islet cell methylome datasets generated by HPAP, a unique resource that provides high-resolution, cell-type-specific epigenomic profiles from human donors across a range of ages and diabetes status^{26,27}. Although previous studies have examined DNAm in whole islets, this dataset enables analysis of epigenetic changes in purified alpha cell and beta cell populations. In an accompanying paper, our colleagues⁵¹ analysed DNAm from sorted human alpha and beta cells and, similar to our findings, identified thousands of DMRs between the two cell types. Remarkably, 66% of the genes associated with DMRs in our study were also associated with DMRs in theirs, despite the differences in experimental and bioinformatics methodologies used, underscoring the robustness of this epigenetic mark.

Using a subset of HPAP donors with alpha and beta cell samples of the highest purity, we traced DNAm changes associated with age and T2D. Our analysis revealed that beta cells, but not alpha cells, from healthy donors undergo progressive demethylation with age at active regulatory regions, particularly at TF-bound *cis*-regulatory elements. This finding is consistent with our previous study in mice⁴⁰, which suggested a conserved adaptive process that supports beta cell function with age. Owing to the limited age range and smaller number of T2D donors, we could not perform an age-related DNAm analysis in T2D. However, a similar demethylation pattern was also noted in T2D compared to CTL donors, suggesting that T2D beta cells may acquire a hypomethylated state earlier in life, consistent with a previous study showing that premature DNA demethylation in peripheral blood leucocytes is associated with increased risk of T2D⁵². Although the changes

are modest in magnitude, they are statistically significant and consistently enriched in functionally relevant regions. The enrichment of hypomethylated regions in regulatory elements suggests a regulated and potentially adaptive process, rather than stochastic drift, targeting loci essential for beta cell identity and function.

DNAm patterns in differentiated cells are generally stable and maintained by the coordinated activity of the maintenance methyltransferase DNMT1 together with DNMT3A, which, although traditionally described as a *de novo* methyltransferase, has been recently shown to also contribute to maintenance methylation^{30,31,53–55}. However, these patterns can be actively remodelled by TET enzymes, which oxidize 5-methylcytosine (5mC) to 5-hydroxymethylcytosine (5hmC). This intermediate can either initiate active or passive demethylation or persist as a stable epigenetic mark, especially in the context of ageing and disease⁵⁶. Importantly, TET-mediated demethylation accumulates at active regulatory regions and TF binding sites^{28,57}, where it may counteract DNMT activity and protect enhancers from repressive methylation^{28,29,58}. In beta cells, such mechanisms could help sustain enhancer activity and support functionality throughout life. Our findings support this idea, as we show that beta-cell-specific gene sets are preferentially hypomethylated, and that core identity genes such as *PDX1*, *MAFA*, *FOXA2* and *ABCC8*, which are associated with hypomethylation, maintain stable expression levels throughout life and in T2D. By contrast, other pathways not enriched near hypomethylated regions, such as those involved in mitochondrial metabolism, oxidative stress defence and secretory processes, tend to show reduced expression in T2D, suggesting that in beta cells, demethylation in regulatory regions primarily serves to preserve stable expression of the identity gene program rather than drive broad transcriptional activation. Alternatively, or in addition, the observed demethylation may result from rare replication events triggered by increased metabolic demand throughout life and under diabetic conditions, during which 5hmC-modified sites are not recognized by DNMT1, leading to a loss of CpG methylation in the daughter cells. However, alpha cells, which have been reported to proliferate at a higher rate in T2D²³, do not show substantial hypomethylation, suggesting that replication-dependent passive demethylation alone is insufficient to explain the beta-cell-specific pattern. Clarifying the relative contributions of these mechanisms will require profiling steady-state 5hmC levels in alpha and beta cells from non-diabetic and diabetic donors. Finally, the expression levels of DNMT1, DNMT3A, DNMT3B and the TET enzymes (TET1–3), which collectively regulate DNA methylation state, remain unchanged with age or in T2D, but are lower in alpha cells than in beta cells.

Beta cell gene expression is influenced by conditions such as endoplasmic reticulum stress, oxidative stress and metabolic workload, and gene activation and repression are often reversible, supporting the adaptive capacity of beta cells until chronic stress overwhelms this capacity, leading to failure and progression to T2D⁵⁹. By contrast, DNAm, being a relatively stable epigenetic mark, may not respond to transient metabolic cues or drive rapid changes in gene expression. Indeed, in our study, most age-related and disease-associated demethylated regions did not strongly correlate with increased expression of nearby genes. Nonetheless, the specific demethylation process observed in beta cells but not alpha cells supports the idea that this represents a cell-type-specific epigenetic adaptation. In beta cells, demethylation may serve to preserve enhancer activity and sustain cellular responsiveness over time, rather than directly modulate gene expression acutely. Based on the fact that we did not detect significant overlap between BMI-demethylated and age-demethylated DMRs, this adaptation is mainly associated with ageing, rather than metabolic stress. Although the functional significance of this age-demethylation remains to be fully elucidated, its cell-type specificity highlights a unique epigenetic adaptive response in this long-lived, metabolically responsive cell type. However, in the context of T2D, this mechanism may ultimately fail, leading to impaired function despite preserved

expression of core identity genes. Future studies should explore whether targeted modulation of the DNAm machinery, particularly TET activity, can enhance beta cell resilience during ageing and diabetes.

Methods

Human pancreatic islets

Pancreatic islets were procured by the HPAP consortium under the Human Islet Research Network (<https://hirnetwork.org>) with approval from the University of Florida Institutional Review Board (201600029) and the United Network for Organ Sharing. A legal representative for each donor provided informed written consent before organ retrieval, and the data have been deidentified. The protocols used for the human islet sorting, whole genome bisulfite sequencing (WGBS), scRNA-seq and snATAC-seq assays used in this work are available on the PancDB website at <https://hpap.pmacs.upenn.edu/explore/workflow/islet-molecular-phenotyping-studies> (see Kaestner lab protocols). In addition to libraries generated with WGBS, the methylome data used in this work also comprises libraries generated using enzymatic methyl sequencing (EM-seq) following these steps: 100 ng DNA input was sheared to 300 bp and cleaned with the Zymo research kit (D4014). Quality control was performed on a BioAnalyzer (Agilent), and EM-seq libraries were generated (New England Biolabs, E7120/E7140). All kits were used following the manufacturer's instructions.

Data analysis

Methylome. All available (154) HPAP methylome samples, regardless of cell type or donor disease state, were pre-processed together (see Extended Data Fig. 9 for workflow outline). Adaptors were trimmed from paired-end reads with cutadapt (v.4.4)⁶⁰. Trimmed reads were aligned to the human hg38, Lambda and pUC19 genomes using bwa-meth (v.0.2.7)⁶¹. The resulting sam files were converted to bam files using samtools (v.1.14)⁶², then duplicated reads were marked by sambamba (v.0.8.1)⁶³ and the resulting bam files were sorted and indexed with samtools. We used wgbstools (v.0.2.0)²⁴ to generate preliminary pat, beta and tab files from the hg38 alignments while removing reads with low mapping quality, duplicated or not mapped in a proper pair (using -F 1796 -q 10). We then leveraged the HPAP whole genome sequencing data to identify the C > T and G > A variants at CpG positions for each donor and subtracted them from the tab files, also using bedtools (v.2.26.0)⁶⁴. Using wgbstools again, we generated beta files from the filtered tab files, then computed average coverage, generated bigwig tracks and segmented the genome using these filtered beta files. In general, the segmentation from wgbstools identifies non-overlapping continuous regions of highly correlated CpG sites similarly methylated in each sample but possibly covarying across conditions. We derived the segmentation from all samples with an average coverage above the median (22×) and required a minimum of four CpGs per region and a max region size of 2,000 bp. This segmentation (2,061,859 regions; median size, 607 bp; median number of CpGs, 8) was then applied to all samples and used in subsequent analyses.

For each sample, we estimated purity using the UXM fragment-level deconvolution algorithm²⁴ (v.0.1.0) with reference Atlas.U25.I4.hg38.full.tsv (from https://github.com/nloyfer/UXM_deconv) restricted to the markers for pancreatic cell types, endothelial cells and monocytes and macrophages. Before applying UXM, we refined the atlas for each donor by filtering out CpG positions where that donor had C > T or G > A variants.

We leveraged methylSig (v.1.11.0)⁶⁵ for differential methylation analyses. We performed several comparisons, including (1) alpha versus beta cells in CTL donors; (2) age (as a numeric covariate) separately in alpha and (3) in beta cells of CTL donors; and (4) T2D versus CTL donors separately for alpha and (5) beta cells. For each comparison, we selected relevant samples with sufficiently high average coverage (~20× or more) and estimated purity (~65% or more). For comparisons between T2D and CTL donors, we selected donors in similar age ranges in the two

groups. The characteristics of the samples used in each comparison are summarized in Supplementary Tables 1–5. For each comparison, we removed CpGs covered by fewer than ten reads in any of the samples and then aggregated methylation fractions by segmentation regions and removed any region covered by fewer than ten reads in any of the samples. We focused on regions that were not on the X and Y chromosomes, with an average methylation difference of at least 5% between the groups being compared. In the case of the age comparisons (where age was treated as a numeric covariate), the two groups used for this filtering were those of donors aged 39–58 years and 18–35 years. To find DMRs, we used the general model test with DSS and a design dependent on the comparison of interest. In comparison (1), we paired by donor; in comparisons (3) to (5), we included ancestry and assay type (WGBS or EM-seq) in the model. In comparison (2), we included assay type in the model but not ancestry, given that the latter was confounded with age. For each comparison, DMRs for further examination were defined based on thresholds for the FDR and effect size; note that effect size here refers to the absolute value of delta, the difference of methylation levels between the two groups as estimated by methylSig (meth_diff). We set basic thresholds of 0.05 for the FDR and 5% for the effect size. But we made either or both of these thresholds more stringent for those comparisons where we expected less subtle differences (also based on inspection of PC and effect size plots), to focus on the top DMRs. The thresholds chosen are listed in Supplementary Table 6.

To functionally annotate DMRs, we defined the following sets of features based on the Gencode Human v43 transcript models:

- 1,500 bp upstream of the transcription start site (TSS);
- 1,501–5,000 bp upstream of TSS;
- 5,001–50,000 bp upstream of TSS;
- 1,000 bp downstream of TSS; and
- 1,001–50,000 bp downstream of TSS and downstream of the transcription end site.

We used bedtools (v.2.26.0)⁶⁴ to mark the features from each of the above sets overlapping with each DMR.

To explore enrichment of signals from alpha, beta and islet-specific snATAC-seq and ChIP-seq experiments, we leveraged EnrichedHeatmap (v.1.32.0)⁶⁶. We downloaded the bigwig files with accessions listed in Supplementary Table 7 from the Common Metabolic Disease Genome Atlas (<https://cmdga.org>). For H3K27me3, we used data from a previous publication⁶⁷, lifted over to hg38 with LiftOver⁶⁸. In addition, we generated bigwig files for chromatin accessibility in alpha and beta cells from HPAP snATAC-seq experiments in CTL and T2D donors as described below. Our plots also leveraged pheatmap (v.1.0.12) (<https://github.com/raivokolde/pheatmap>) and ggplot2 (v.3.5.1)⁶⁹. The principal component analyses leveraged PCATools (v.2.14.0) (<https://bioconductor.org/packages/PCATools>) with removeVar = 0.1.

The analyses of beta cell methylomes from healthy donors with respect to BMI and GSIS were done in the same manner as the age analyses, using methylSig and with assay type and ancestry in the model. BMI (resp. GSIS) was used as a numeric covariate, and the effect size was based on its top and bottom quartiles. GSIS was measured by the insulin ratio B/A derived from the individual perfusion data obtained from PancDB as follows. The numerator, B, was the maximum insulin secretion value after stimulation with G16.7. The denominator, A, was the average insulin secretion over the time points in the 'plateau' amino acid stimulation phase (AAM, before G3 stimulation). For the latter, outlier time points at the beginning of the AAM phase were manually filtered out donor by donor.

As a quality control check, for each of the alpha and beta cell age or T2D versus CTL comparison, we randomly shuffled the sample labels 100 times and ran the same analysis on the shuffled data (summary counts are provided in Supplementary Table 16). For the age comparisons in both cell types and the beta cell T2D comparison, the number of DMRs identified in shuffled data was much reduced (almost null in the

age comparisons) and did not follow the imbalance in hypomethylation versus hypermethylation observed in the unshuffled data.

scRNA-seq. For each donor islet sample, we obtained counts with Cell Ranger (v.7.1.0)⁷⁰ and used Seurat (v.4.9.9.9041)⁷¹ (complemented by SoupX (v.1.6.2)⁷² and scDblFinder (v.1.12.0)⁷³) for clean-up, normalization, pre-processing and data integration. Cells were annotated with two approaches: scSorter (v.0.0.2)⁷⁴ and manual cluster annotation based on selected pancreatic cell markers. Only cells for which the two approaches agreed were assigned to a final cell type.

For each cell type, we used all available relevant donors for a comparison of interest, with at least 100 cells of that type and processed with SC3Pv3 chemistry. We generated pseudo-bulk counts and used DESeq2 (v.1.38.1) for differential expression analyses⁷⁵. For the age comparison, we did not treat age as a numeric covariate as we did for DMRs, but we compared age group categories (18–35 vs 39–58 years old) based on DESeq2 recommended guidelines.

snATAC-Seq profiles in alpha and beta cells. Chromatin accessibility profiles for alpha and beta cells were generated using HPAP snATAC-seq datasets. Each dataset was first analysed using Signac (v.1.7.0)⁷⁶ and Seurat (v.4.4.0)⁷¹. A standard processing pipeline was applied (https://stuartlab.org/signac/articles/pbmc_vignette). Nuclei with fewer than 1,000 or more than 100,000 reads in peaks, a TSS enrichment score of <1 or a nucleosome signal of >2 were filtered out. Each nucleus was annotated by mapping to an internal multiome reference dataset, and nuclei with a mapping score of >0.8 were kept.

Then, to generate cell-type-specific tracks in each disease group, we used samples from CTL donors with age ≥ 30 years and samples from T2D donors. With cell types annotated from the previous steps, fragments associated with cells from each donor and each cell type (alpha and beta) were merged to generate pseudo-bulk tracks; tracks with fewer than 30 cells were removed. A bed file including the start, end and chromosome information of each read was created for each donor and each cell type. Bam files were constructed using bedToBam (v.2.30.0)⁶⁴ with a genome size file provided as part of the GRCh38 reference – 2020-A-2.0.0 available on the 10x Genomics website (<https://cf.10xgenomics.com/supp/cell-arc/refdata-cellranger-arc-GRCh38-2020-A-2.0.0.tar.gz>). Bam files were indexed using samtools (v.1.11 index)⁶². BAMscale (v.0.0.5)⁷⁷ was used to generate scaled coverage tracks, with parameter -t 4. Lastly, to generate cell-type-specific tracks per disease group, cell-type-specific tracks were merged across donors of the same condition using bigWigMerge (v.2) and the output was sorted and converted to a bigwig file using bedGraphToBigWig (v.2.8)⁷⁸.

Gene set analyses. To analyse enrichment of gene sets associated with DNAm changes, we focused on a gene set collection comprising gene sets obtained from MSigDB⁷⁹ and custom gene sets defined in a previous publication¹³. The hypothesis-driven gene set collection is described in Supplementary Table 8. For these analyses, we used the top DMRs (in terms of effect size) to reduce noise and focus on the most robust enrichment. For the comparison between alpha and beta cells, we used a $|\text{delta}| > 40\%$ cutoff owing to the large inherent differences between these two cell types, whereas for all other comparisons (age and T2D), we used a consistent $|\text{delta}| > 10\%$ cutoff. We used a hypergeometric test implemented in the Genomica (v.3.0.0) software⁸⁰, considering gene sets with $P < 0.01$ and $\text{FDR} < 0.05$ to be significant. For the association of genes to DMRs in likely enhancers, we used protein-coding genes in the unions of the following DMR annotation files defined above: 1,501–50,000 bp upstream of TSS or 1,001–50,000 bp downstream of TSS and downstream of the transcription end site. We refer to these genes as 'DMR-distal'.

To analyse enrichment of gene sets associated with mRNA expression, we used GSEA^{79,81} (v.4.3.3) on the DESeq2 normalized scRNA-seq

pseudo-bulk counts. The gene sets input in these analyses were the Hallmark gene sets from MSigDB, to cover the main biological programmes.

T2D GWAS SNP enrichment analyses. To examine the 558 T2D-associated SNPs identified in a previous publication⁵⁰ versus the 8,619 beta cell demethylated DMRs in T2D, we used GREGOR (v.1.4.0)⁸² after lifting these regions over to hg19. We used default parameter settings, a threshold of $r^2 = 0.7$ for proxies and EUR as the reference population (given that most of the donors in this comparison were from this ancestry).

Reporting summary

Further information on research design is available in the Nature Portfolio Reporting Summary linked to this article.

Data availability

Raw data and metadata related to this work are available on the PancDB website <https://hpap.pmacs.upenn.edu> and on dbGaP (<https://www.ncbi.nlm.nih.gov/gap>) with accession no. phs002465 (v.2). With the PancDB website interactive analysis link, it is also possible to explore Genome Browser tracks for our methylation data, as well as the results of islet perfusion experiments used in our insulin secretion ratio calculations. Finally, the result files for the methylome comparisons in this work and the scRNA-seq DESeq2 results are available in the Supplementary Data.

Code availability

The study was conducted using only publicly available software as outlined above; no new code was generated. The list of software packages and versions used is also available in the Nature Portfolio Reporting Summary linked to this article.

References

- Al-Khelaifi, F. et al. Metabolic GWAS of elite athletes reveals novel genetically-influenced metabolites associated with athletic performance. *Sci Rep.* **9**, 19889 (2019).
- Kresnajati, S. et al. Changes in arterial stiffness in response to various types of exercise modalities: a narrative review on physiological and endothelial senescence perspectives. *Cells* **11**, 3544 (2022).
- Pontzer, H. et al. Daily energy expenditure through the human life course. *Science* **373**, 808–812 (2021).
- Chang-Chen, K. J., Mullur, R. & Bernal-Mizrachi, E. Beta-cell failure as a complication of diabetes. *Rev. Endocr. Metab. Disord.* **9**, 329–343 (2008).
- Cefalu, W. T. et al. Contribution of visceral fat mass to the insulin resistance of aging. *Metabolism* **44**, 954–959 (1995).
- Iozzo, P. et al. Independent influence of age on basal insulin secretion in nondiabetic humans. European Group for the Study of Insulin Resistance. *J. Clin. Endocrinol. Metab.* **84**, 863–868 (1999).
- Arrojo, E. D. R. et al. Age mosaicism across multiple scales in adult tissues. *Cell Metab.* **30**, 343–351.e3 (2019).
- Cnop, M. et al. The long lifespan and low turnover of human islet beta cells estimated by mathematical modelling of lipofuscin accumulation. *Diabetologia* **53**, 321–330 (2010).
- Perl, S. et al. Significant human beta-cell turnover is limited to the first three decades of life as determined by in vivo thymidine analog incorporation and radiocarbon dating. *J. Clin. Endocrinol. Metab.* **95**, E234–E239 (2010).
- Wang, Y. J. et al. Single-cell mass cytometry analysis of the human endocrine pancreas. *Cell Metab.* **24**, 616–626 (2016).
- Castell, A. L. et al. β Cell mass expansion during puberty involves serotonin signaling and determines glucose homeostasis in adulthood. *JCI Insight* **7**, e160854 (2022).
- Rieck, S. & Kaestner, K. H. Expansion of β -cell mass in response to pregnancy. *Trends Endocrinol. Metab.* **21**, 151–158 (2010).
- Avrahami, D. et al. Single-cell transcriptomics of human islet ontogeny defines the molecular basis of β -cell dedifferentiation in T2D. *Mol. Metab.* **42**, 101057 (2020).
- Shrestha, S. et al. Aging compromises human islet beta cell function and identity by decreasing transcription factor activity and inducing ER stress. *Sci. Adv.* **8**, eabo3932 (2022).
- Bergman, Y. & Cedar, H. DNA methylation dynamics in health and disease. *Nat. Struct. Mol. Biol.* **20**, 274–281 (2013).
- Horvath, S. & Raj, K. DNA methylation-based biomarkers and the epigenetic clock theory of ageing. *Nat. Rev. Genet.* **19**, 371–384 (2018).
- Das, P. M. & Singal, R. DNA methylation and cancer. *J. Clin. Oncol.* **22**, 4632–4642 (2004).
- Volkov, P. et al. Whole-genome bisulfite sequencing of human pancreatic islets reveals novel differentially methylated regions in type 2 diabetes pathogenesis. *Diabetes* **66**, 1074–1085 (2017).
- Dayeh, T. et al. Genome-wide DNA methylation analysis of human pancreatic islets from type 2 diabetic and non-diabetic donors identifies candidate genes that influence insulin secretion. *PLoS Genet.* **10**, e1004160 (2014).
- Ronn, T. et al. Genes with epigenetic alterations in human pancreatic islets impact mitochondrial function, insulin secretion, and type 2 diabetes. *Nat. Commun.* **14**, 8040 (2023).
- Henquin, J. C. & Rahier, J. Pancreatic alpha cell mass in European subjects with type 2 diabetes. *Diabetologia* **54**, 1720–1725 (2011).
- Wu, M. et al. Single-cell analysis of the human pancreas in type 2 diabetes using multi-spectral imaging mass cytometry. *Cell Rep.* **37**, 109919 (2021).
- Yoon, K. H. et al. Selective β -cell loss and α -cell expansion in patients with type 2 diabetes mellitus in Korea. *J. Clin. Endocrinol. Metab.* **88**, 2300–2308 (2003).
- Loyfer, N. et al. A DNA methylation atlas of normal human cell types. *Nature* **613**, 355–364 (2023).
- Drawshy, Z. et al. DNA methylation-based assessment of cell composition in human pancreas and islets. *Diabetes* **73**, 554–564 (2024).
- Kaestner, K. H., Powers, A. C., Naji, A., Consortium, H. & Atkinson, M. A. NIH initiative to improve understanding of the pancreas, islet, and autoimmunity in type 1 diabetes: The Human Pancreas Analysis Program (HPAP). *Diabetes* **68**, 1394–1402 (2019).
- Shapira, S. N., Naji, A., Atkinson, M. A., Powers, A. C. & Kaestner, K. H. Understanding islet dysfunction in type 2 diabetes through multidimensional pancreatic phenotyping: The Human Pancreas Analysis Program. *Cell Metab.* **34**, 1906–1913 (2022).
- Hon, G. C. et al. 5mC oxidation by Tet2 modulates enhancer activity and timing of transcriptome reprogramming during differentiation. *Mol Cell.* **56**, 286–297 (2014).
- Stefansson, O. A. et al. The correlation between CpG methylation and gene expression is driven by sequence variants. *Nat. Genet.* **56**, 1624–1631 (2024).
- Li, E., Bestor, T. H. & Jaenisch, R. Targeted mutation of the DNA methyltransferase gene results in embryonic lethality. *Cell* **69**, 915–926 (1992).
- Lei, H. et al. De novo DNA cytosine methyltransferase activities in mouse embryonic stem cells. *Development* **122**, 3195–3205 (1996).
- Pasquali, L. et al. Pancreatic islet enhancer clusters enriched in type 2 diabetes risk-associated variants. *Nat. Genet.* **46**, 136–143 (2014).
- Neiman, D. et al. Islet cells share promoter hypomethylation independently of expression, but exhibit cell-type-specific methylation in enhancers. *Proc. Natl Acad. Sci. USA* **114**, 13525–13530 (2017).

34. Hamilton, A. et al. Adrenaline stimulates glucagon secretion by Tpc2-dependent Ca^{2+} mobilization from acidic stores in pancreatic α -cells. *Diabetes* **67**, 1128–1139 (2018).
35. Wortham, M. & Sander, M. Mechanisms of β -cell functional adaptation to changes in workload. *Diabetes Obes. Metab.* **18**, 78–86 (2016).
36. Enge, M. et al. Single-cell analysis of human pancreas reveals transcriptional signatures of aging and somatic mutation patterns. *Cell* **171**, 321–330.e14 (2017).
37. Tserel, L. et al. Age-related profiling of DNA methylation in CD8⁺ T cells reveals changes in immune response and transcriptional regulator genes. *Sci. Rep.* **5**, 13107 (2015).
38. Tong, H. et al. Cell-type specific epigenetic clocks to quantify biological age at cell-type resolution. *Aging (Albany NY)* **16**, 13452–13504 (2024).
39. Gontier, G. et al. Tet2 rescues age-related regenerative decline and enhances cognitive function in the adult mouse brain. *Cell Rep.* **22**, 1974–1981 (2018).
40. Avrahami, D. et al. Aging-dependent demethylation of regulatory elements correlates with chromatin state and improved β cell function. *Cell Metab.* **22**, 619–632 (2015).
41. Dorrell, C. et al. Human islets contain four distinct subtypes of β cells. *Nat. Commun.* **7**, 11756 (2016).
42. Dror, E. et al. Epigenetic dosage identifies two major and functionally distinct β cell subtypes. *Cell Metab.* **35**, 821–836.e7 (2023).
43. Brooks, E. P. et al. NKX2.2 and KLF4 cooperate to regulate α -cell identity. *Genes Dev.* **39**, 242–260 (2025).
44. Gao, N. et al. Foxa1 and Foxa2 maintain the metabolic and secretory features of the mature β -cell. *Mol. Endocrinol.* **24**, 1594–1604 (2010).
45. Gao, N. et al. Foxa2 controls vesicle docking and insulin secretion in mature β cells. *Cell Metab.* **6**, 267–279 (2007).
46. Lee, C. S., Sund, N. J., Behr, R., Herrera, P. L. & Kaestner, K. H. Foxa2 is required for the differentiation of pancreatic α -cells. *Dev. Biol.* **278**, 484–495 (2005).
47. Pullen, T. J. & Rutter, G. A. When less is more: the forbidden fruits of gene repression in the adult β -cell. *Diabetes Obes. Metab.* **15**, 503–512 (2013).
48. Fang, Z. et al. Single-cell heterogeneity analysis and CRISPR screen identify key β -cell-specific disease genes. *Cell Rep.* **26**, 3132–3144.e7 (2019).
49. Segerstolpe, A. et al. Single-cell transcriptome profiling of human pancreatic islets in health and type 2 diabetes. *Cell Metab.* **24**, 593–607 (2016).
50. Vujkovic, M. et al. Discovery of 318 new risk loci for type 2 diabetes and related vascular outcomes among 1.4 million participants in a multi-ancestry meta-analysis. *Nat. Genet.* **52**, 680–691 (2020).
51. Ofori, J. K. et al. Cell-specific DNA methylation in human α - and β -cells regulates gene expression in type 2 diabetes. *Nat. Metab.* <https://doi.org/10.1038/s42255-026-01498-9> (2026).
52. Toperoff, G. et al. Premature aging of leukocyte DNA methylation is associated with type 2 diabetes prevalence. *Clin. Epigenetics* **7**, 35 (2015).
53. Feng, J. et al. Dnmt1 and Dnmt3a maintain DNA methylation and regulate synaptic function in adult forebrain neurons. *Nat. Neurosci.* **13**, 423–430 (2010).
54. Jeong, S. et al. Selective anchoring of DNA methyltransferases 3A and 3B to nucleosomes containing methylated DNA. *Mol. Cell Biol.* **29**, 5366–5376 (2009).
55. Xu, Z. et al. Regulation of de novo and maintenance DNA methylation by DNA methyltransferases in postimplantation embryos. *J. Biol. Chem.* **301**, 107990 (2025).
56. Bachman, M. et al. 5-Hydroxymethylcytosine is a predominantly stable DNA modification. *Nat. Chem.* **6**, 1049–1055 (2014).
57. Schubeler, D. Function and information content of DNA methylation. *Nature* **517**, 321–326 (2015).
58. Charlton, J. et al. TETs compete with DNMT3 activity in pluripotent cells at thousands of methylated somatic enhancers. *Nat. Genet.* **52**, 819–827 (2020).
59. Chen, C. W. et al. Adaptation to chronic ER stress enforces pancreatic β -cell plasticity. *Nat. Commun.* **13**, 4621 (2022).
60. Martin, M. Cutadapt removes adapter sequences from high-throughput sequencing reads. *EMBnet J.* **17**, 10–12 (2011).
61. Pedersen, B. S., Eyring, K., De, S., Yang, I. V. & Schwartz, D. A. Fast and accurate alignment of long bisulfite-seq reads. Preprint at <https://arxiv.org/abs/1401.1129> (2014).
62. Danecek, P. et al. Twelve years of SAMtools and BCFtools. *Gigascience* **10**, giab008 (2021).
63. Tarasov, A., Vilella, A. J., Cuppen, E., Nijman, I. J. & Prins, P. Sambamba: fast processing of NGS alignment formats. *Bioinformatics* **31**, 2032–2034 (2015).
64. Quinlan, A. R. & Hall, I. M. BEDTools: a flexible suite of utilities for comparing genomic features. *Bioinformatics* **26**, 841–842 (2010).
65. Park, Y., Figueroa, M. E., Rozek, L. S. & Sartor, M. A. MethylSig: a whole genome DNA methylation analysis pipeline. *Bioinformatics* **30**, 2414–2422 (2014).
66. Gu, Z., Eils, R., Schlesner, M. & Ishaque, N. EnrichedHeatmap: an R/Bioconductor package for comprehensive visualization of genomic signal associations. *BMC Genomics* **19**, 234 (2018).
67. Bramswig, N. C. et al. Epigenomic plasticity enables human pancreatic α to β cell reprogramming. *J. Clin. Invest.* **123**, 1275–1284 (2013).
68. Hinrichs, A. S. et al. The UCSC Genome Browser Database: update 2006. *Nucleic Acids Res.* **34**, D590–D598 (2006).
69. Wickham, H. *ggplot2: Elegant Graphics for Data Analysis* (Springer, 2016).
70. Zheng, G. X. et al. Massively parallel digital transcriptional profiling of single cells. *Nat. Commun.* **8**, 14049 (2017).
71. Hao, Y. et al. Integrated analysis of multimodal single-cell data. *Cell* **184**, 3573–3587.e29 (2021).
72. Young, M. D. & Behjati, S. SoupX removes ambient RNA contamination from droplet-based single-cell RNA sequencing data. *Gigascience* **9**, g1aa151 (2020).
73. Germain, P. L., Lun, A., Garcia Meixide, C., Macnair, W. & Robinson, M. D. Doublet identification in single-cell sequencing data using scDblFinder. *F1000Res* **10**, 979 (2021).
74. Guo, H. & Li, J. scSorter: assigning cells to known cell types according to marker genes. *Genome Biol.* **22**, 69 (2021).
75. Love, M. I., Huber, W. & Anders, S. Moderated estimation of fold change and dispersion for RNA-seq data with DESeq2. *Genome Biol.* **15**, 550 (2014).
76. Stuart, T., Srivastava, A., Madad, S., Lareau, C. A. & Satija, R. Single-cell chromatin state analysis with Signac. *Nat. Methods* **18**, 1333–1341 (2021).
77. Pongor, L. S. et al. BAMscale: quantification of next-generation sequencing peaks and generation of scaled coverage tracks. *Epigenetics Chromatin* **13**, 21 (2020).
78. Kent, W. J., Zweig, A. S., Barber, G., Hinrichs, A. S. & Karolchik, D. BigWig and BigBed: enabling browsing of large distributed datasets. *Bioinformatics* **26**, 2204–2207 (2010).
79. Subramanian, A. et al. Gene set enrichment analysis: a knowledge-based approach for interpreting genome-wide expression profiles. *Proc. Natl Acad. Sci. USA* **102**, 15545–15550 (2005).
80. Segal, E. et al. Module networks: identifying regulatory modules and their condition-specific regulators from gene expression data. *Nat. Genet.* **34**, 166–176 (2003).
81. Mootha, V. K. et al. PGC-1 α -responsive genes involved in oxidative phosphorylation are coordinately downregulated in human diabetes. *Nat. Genet.* **34**, 267–273 (2003).

82. Schmidt, E. M. et al. GREGOR: evaluating global enrichment of trait-associated variants in epigenomic features using a systematic, data-driven approach. *Bioinformatics* **31**, 2601–2606 (2015).

Acknowledgements

We thank the families of the organ donors and the entire HPAP team for making this study possible. We used data acquired from the HPAP (HPAP-RRID:SCR_016202) database (<https://hpap.pmacs.upenn.edu>), a Human Islet Research Network (RRID:SCR_014393) consortium supported by NIDDK grants UC4-DK-112217, U01-DK-123594, UC4-DK-112232 and U01-DK-123716. Further support was provided by NIDDK grant U01-DK-134995 to D.A., B.G. and K.H.K. B.G. and D.A. are supported by grants from the Israel Science Foundation and JDRF (1782/18 and 2982/20), the US–Israel Binational Science Foundation (2019314) and the EU's Horizon 2020 research and innovation program no. 874710. D.A. is supported by the Israel Science Foundation (2166/24). The funders had no role in study design, data collection and analysis, decision to publish or preparation of the manuscript. Finally, we thank the editor and reviewers for their constructive comments and suggestions.

Author contributions

D.A. and K.H.K. conceived and supervised this work. B.G. provided conceptual input. E.M., D.A. and K.H.K. wrote the manuscript. E.M. pre-processed the data, performed most computational analyses and uploaded the data to PancDB and dbGaP. H.C.D. performed human islet sorting, prepared and sequenced the EM-seq, scRNA-seq and snATAC-seq libraries, performed PC analyses and contributed to data interpretation and manuscript outline. D.A. performed gene set analyses and GSEA. J.L. prepared the WGBS libraries. J.S. oversaw the sequencing, provided feedback and helped with data uploads to PancDB and dbGaP. T.D., D.L., D.B. and H.E.-M. contributed to human islet sorting and generated scRNA-seq and snATAC-seq libraries. M.L. performed the snATAC-seq analyses. C.L. and A.N. performed islet isolation from donor tissues. E.F. performed additional biological analyses. All authors reviewed and approved the manuscript.

Competing interests

The authors declare no competing interests.

Additional information

Extended data is available for this paper at <https://doi.org/10.1038/s42255-026-01495-y>.

Supplementary information The online version contains supplementary material available at <https://doi.org/10.1038/s42255-026-01495-y>.

Correspondence and requests for materials should be addressed to Klaus H. Kaestner or Dana Avrahami.

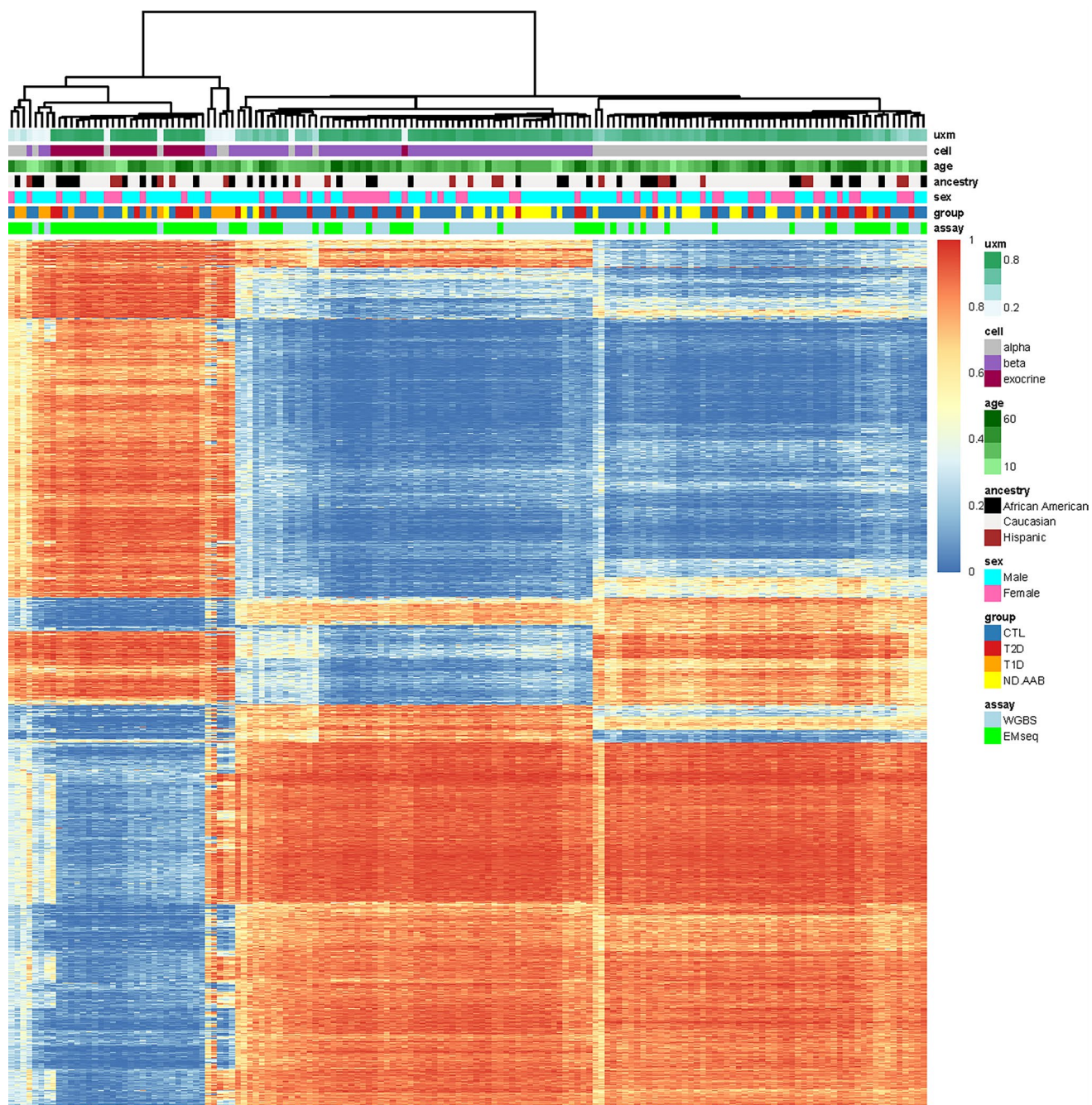
Peer review information *Nature Metabolism* thanks Guoqiang Gu and the other, anonymous, reviewer(s) for their contribution to the peer review of this work. Primary Handling Editor: Revati Dewal, in collaboration with the *Nature Metabolism* team.

Reprints and permissions information is available at www.nature.com/reprints.

Publisher's note Springer Nature remains neutral with regard to jurisdictional claims in published maps and institutional affiliations.

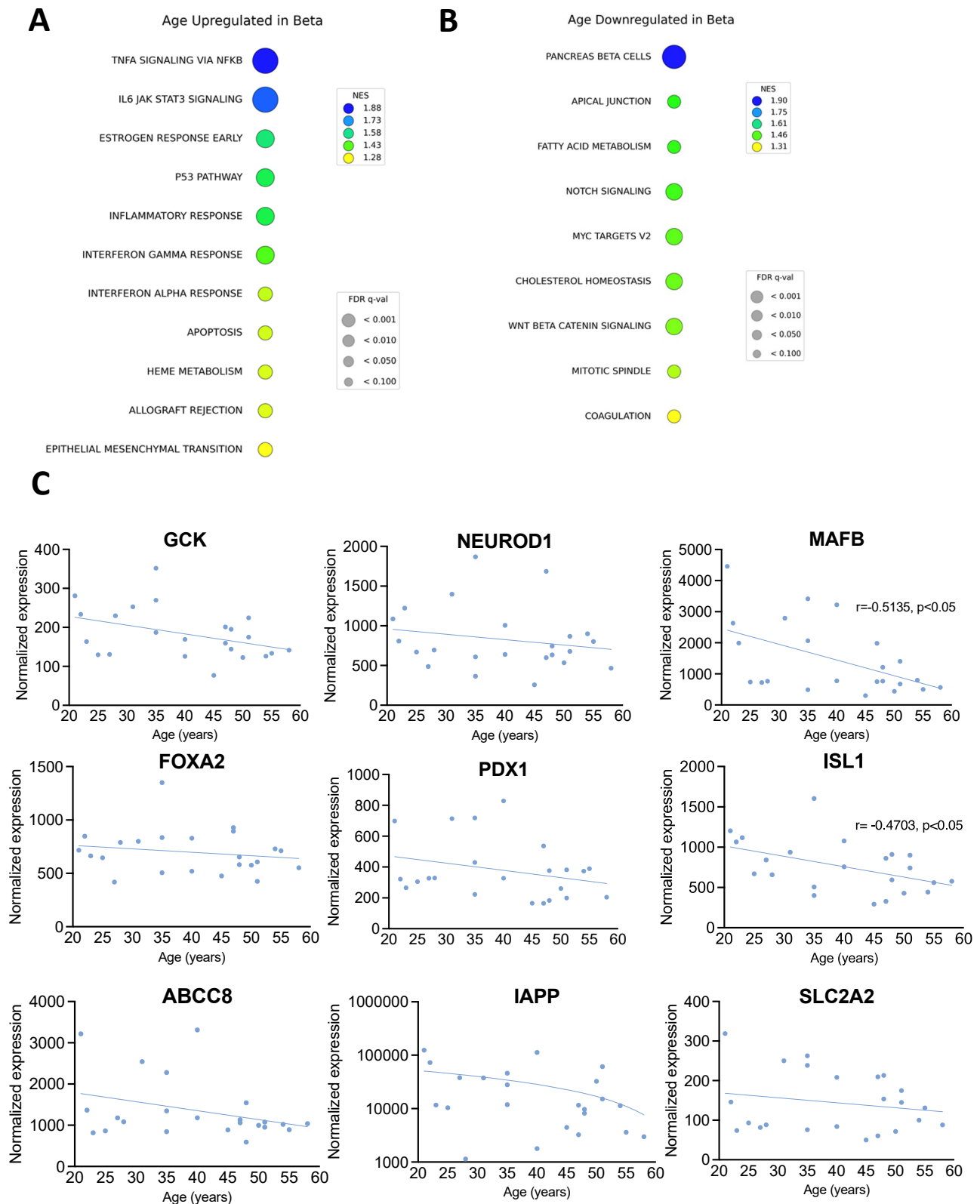
Open Access This article is licensed under a Creative Commons Attribution-NonCommercial-NoDerivatives 4.0 International License, which permits any non-commercial use, sharing, distribution and reproduction in any medium or format, as long as you give appropriate credit to the original author(s) and the source, provide a link to the Creative Commons licence, and indicate if you modified the licensed material. You do not have permission under this licence to share adapted material derived from this article or parts of it. The images or other third party material in this article are included in the article's Creative Commons licence, unless indicated otherwise in a credit line to the material. If material is not included in the article's Creative Commons licence and your intended use is not permitted by statutory regulation or exceeds the permitted use, you will need to obtain permission directly from the copyright holder. To view a copy of this licence, visit <http://creativecommons.org/licenses/by-nc-nd/4.0/>.

© The Author(s) 2026



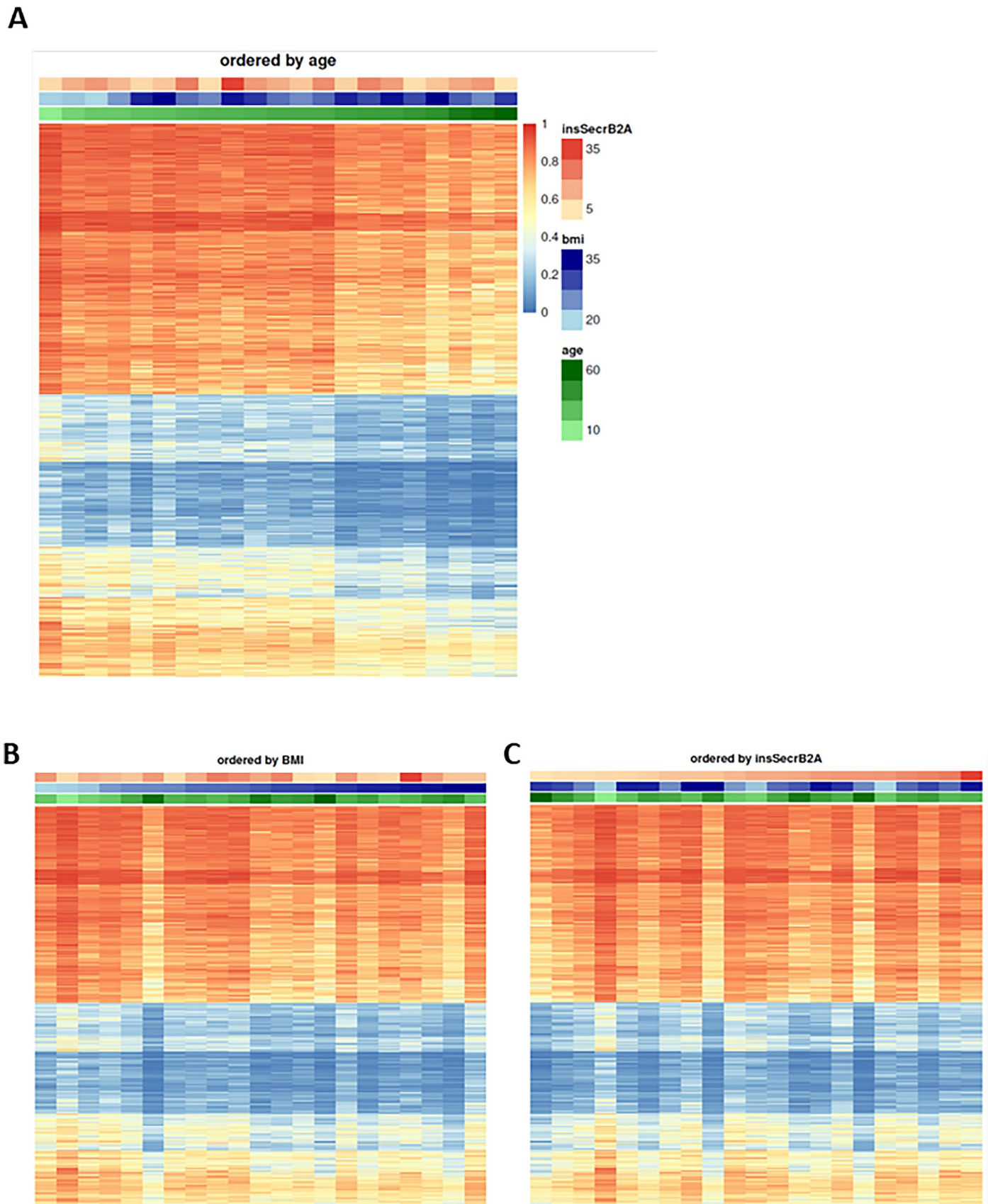
Extended Data Fig. 1 | QC clustering. Quality control clustering of all 154 HPAP methylome samples. Rows represent the top 1% most variable segmentation regions (18,972) on chromosomes other than X and Y. Columns correspond to samples. Rows and columns are clustered using Manhattan distance as similarity

metrics. Horizontal bars at the top indicate values of several covariates for each sample. uxm=UXM estimated purity score, ND.AAB= non-diabetic auto-antibody positive.



Extended Data Fig. 2 | Beta cell scRNA-Seq data across age. MSigDB Hallmark gene sets identified by GSEA as (a) up-regulated with age and (b) down-regulated with age in beta cells from CTL donors. (c) DESeq2 normalized expression (from pseudo-bulk counts) of selected genes across age. Unadjusted two-sided Pearson

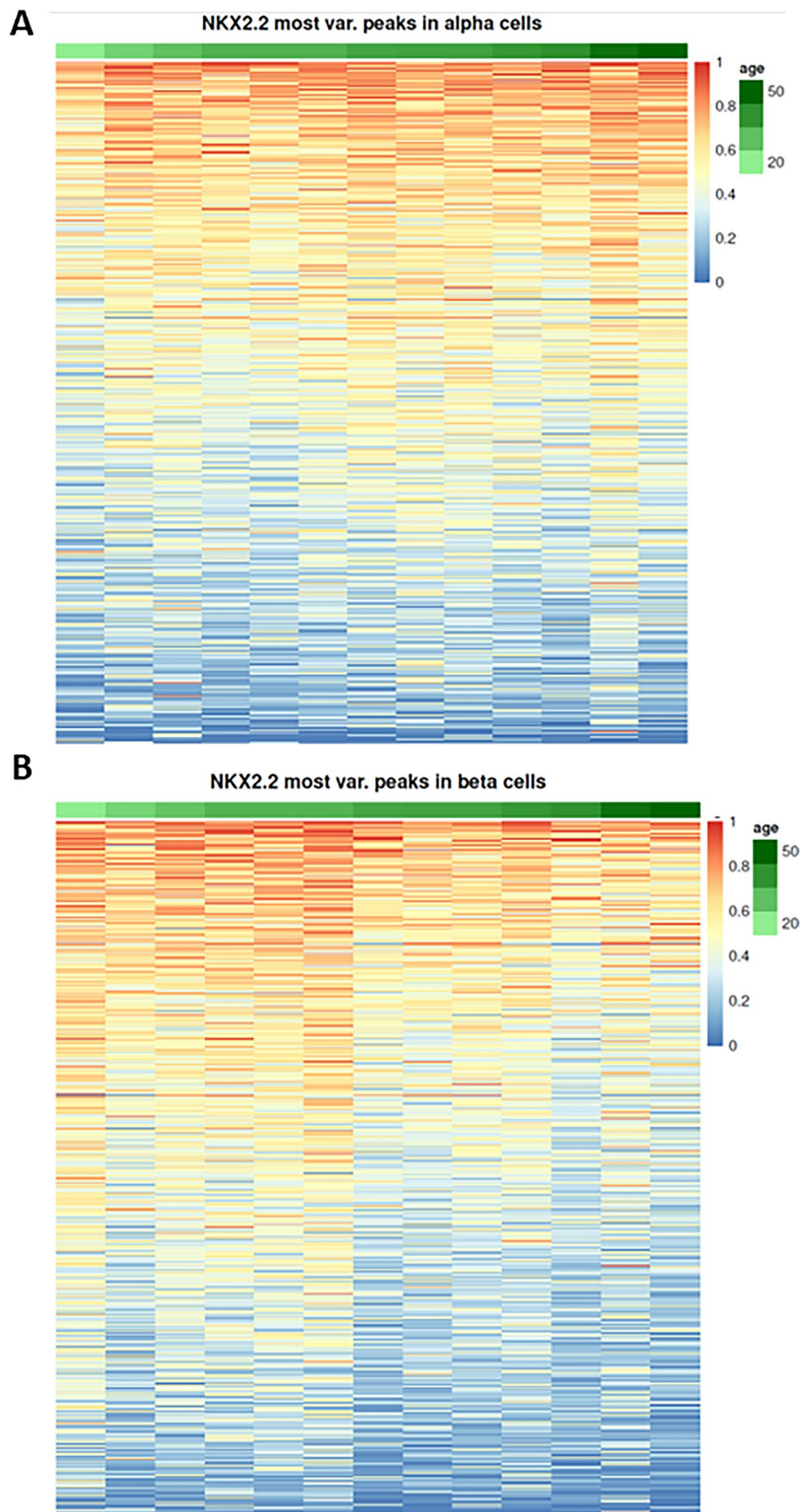
correlation p-values: *GCK* ($p = 0.05$), *NEUROD1* ($p = 0.36$), *MAFB* ($p = 0.01$), *FOXA2* ($p = 0.40$), *PDX1* ($p = 0.19$), *ISL1* ($p = 0.02$), *ABCC8* (0.11), *IAPP* ($p = 0.06$), and *SLC2A2* ($p = 0.38$).



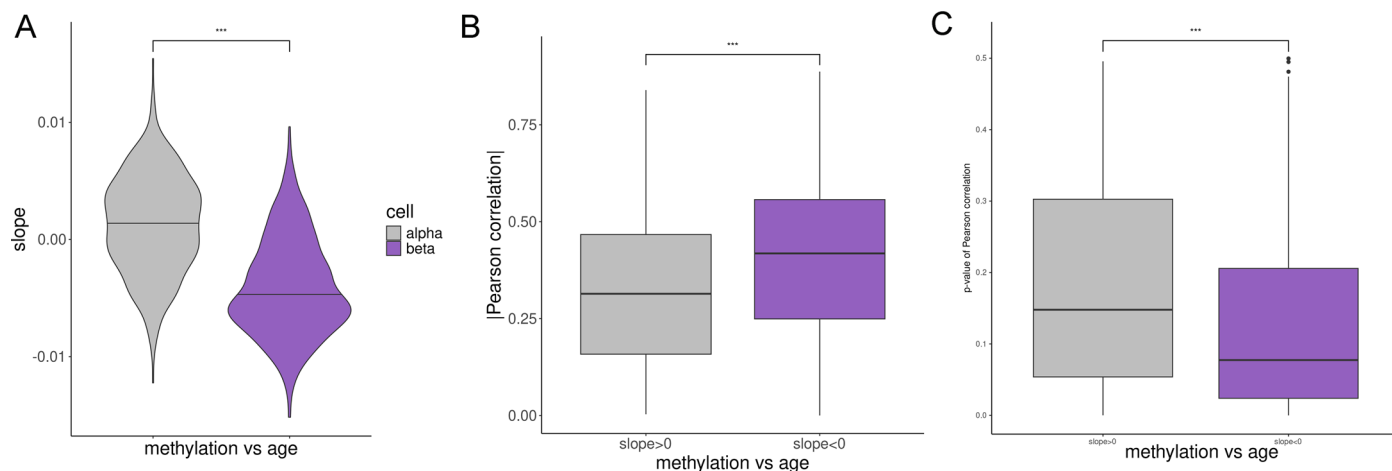
Extended Data Fig. 3 | Heatmaps of beta cell age DMRs. Heatmaps of average methylation of the age-hypomethylated DMRs in beta cells of CTL donors, ordered by (a) age, (b) BMI, and (c) GSIS respectively. GSIS was measured by the insulin secretion ratio (insSecrB2A) described in Methods. The top bars indicate the age, BMI, and insSecrB2A values for each donor.

Extended Data Fig. 4 | Enrichment heatmaps for alpha cells DMRs. Enrichment plot of signals from (a) islet histone modifications ChIP-Seq and from (b) snATAC-Seq in alpha cells and islet TF ChIP-Seq experiments for the 1,466 age-associated DMRs with $FDR < 0.01$ and $|\Delta| > 5\%$ in alpha cells from CTL donors. Each row

shows the signal plotted over the 10 kb region centered at one DMR. Top: regions hypermethylated in younger alpha cells; bottom: regions hypermethylated in older alpha cells.

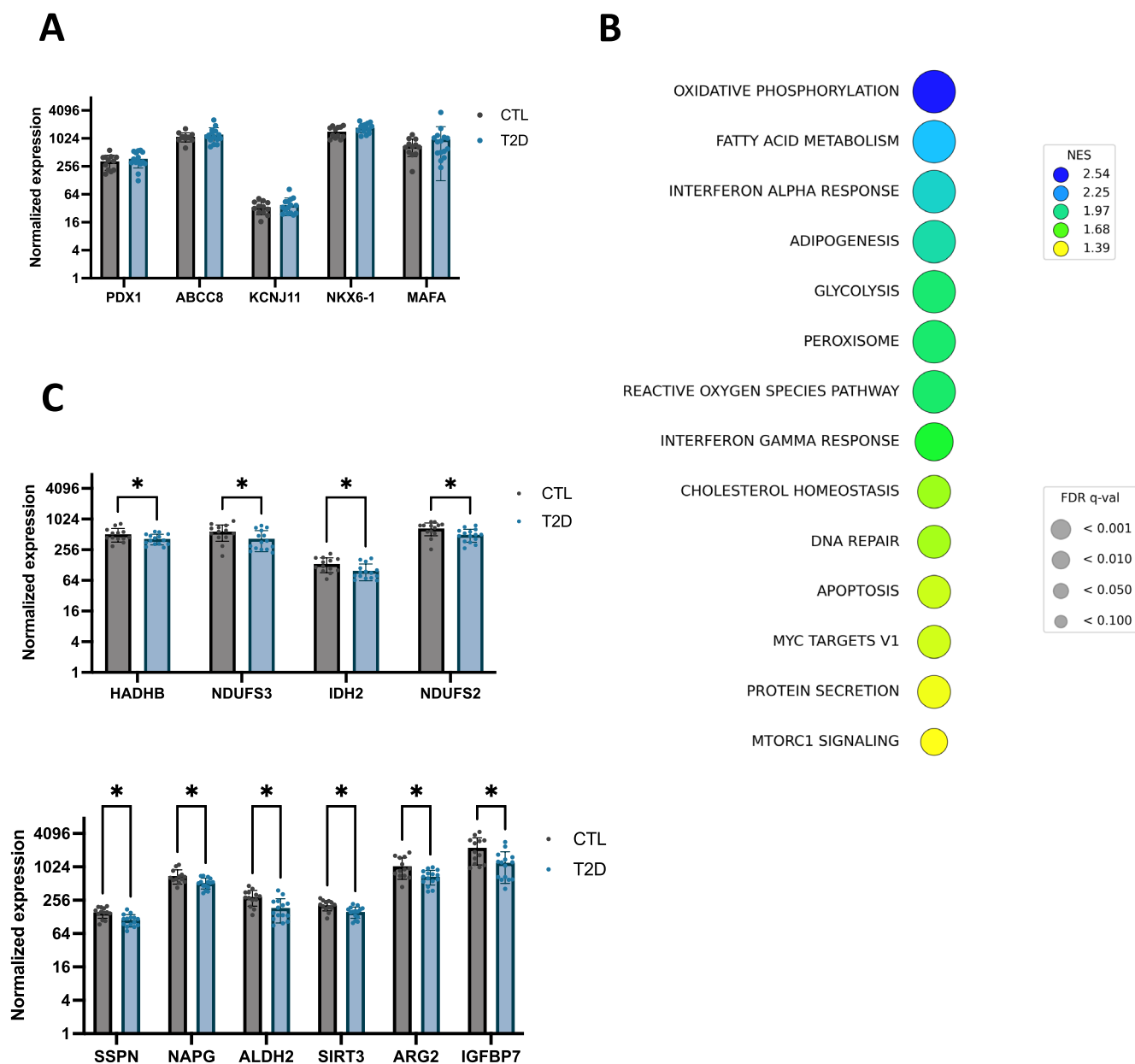


Extended Data Fig. 5 | NKX2.2 binding sites methylation heatmaps. Heatmaps of average methylation for NKX2.2 peaks³² for (a) alpha and (b) beta cells. Shown are the 500 most variable peaks (separately, for each cell type) across 13 age-matched donors.



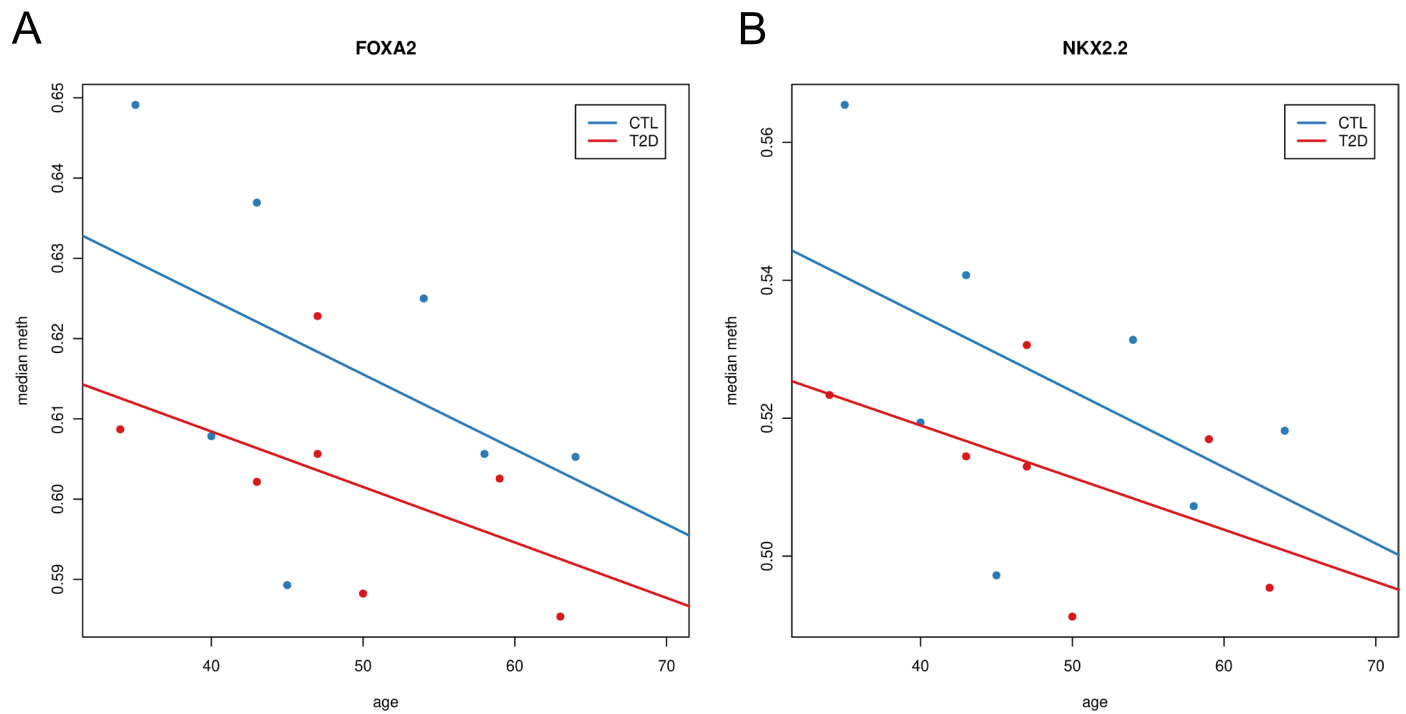
Extended Data Fig. 6 | Linear fit slopes and Pearson correlations for *NKX2.2* binding sites. (a) Violin plots of the slopes of linear fits to methylation versus age corresponding to the regions from Extended Data Fig. 5 in the two cell types. Boxplots of (b) absolute Pearson correlation coefficients and (c) Pearson correlation p-values (for positive association in alpha cells and negative association in beta cells) of methylation versus age at the 306 regions with slope

> 0 in alpha cells and the 408 regions with slope < 0 in beta cells from Extended Data Fig. 5. Boxplots description: middle line=median; box upper (resp. lower) bound=3rd (resp. 1st) quartile; upper/lower whisker extends to the largest/smallest value within 1.5×IQR; individual points=outliers. The asterisks indicate a two-sided Wilcoxon p-value < 0.001 ($p < 2.22 \times 10^{-16}$ for (a), $p = 2.6 \times 10^{-8}$ for (b) and (c)).

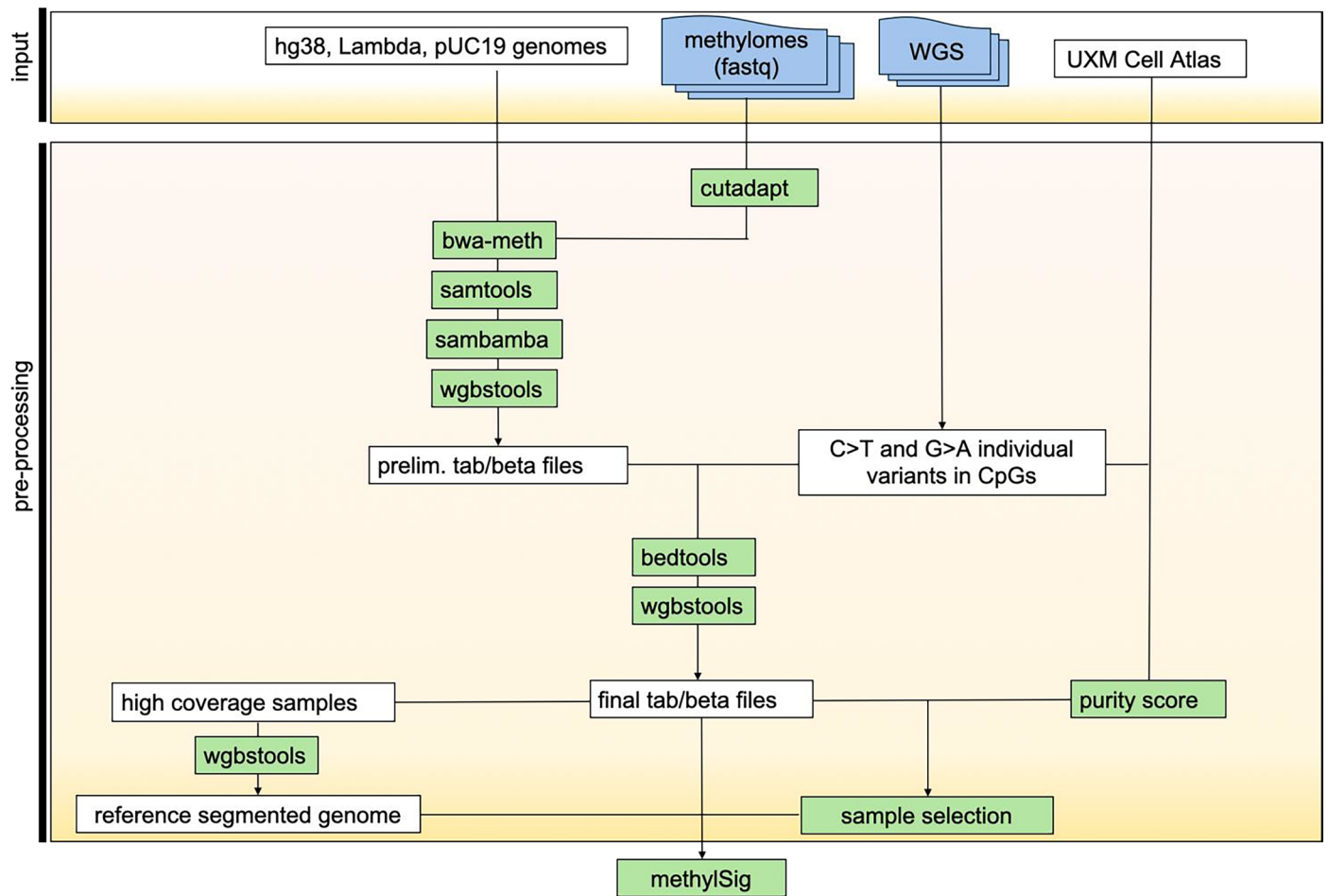


Extended Data Fig. 7 | Beta cell scRNA-Seq data in T2D and CTL. (a) DESeq2 normalized expression (from pseudo-bulk counts) of key beta cell identity genes in CTL (n = 13) and T2D (n = 15) donors of similar age from HPAP scRNA-Seq data, showing stable expression in T2D beta cells. Data are presented as mean values

+/- SD. (b) MSigDB Hallmark gene sets identified by GSEA as down-regulated in beta cells from T2D donors compared with CTLs. (c) DESeq2 normalized expression (from pseudo-bulk counts) of selected genes from broader functional pathways for the same donors as (a). Data are presented as mean values +/- SD.



Extended Data Fig. 8 | Beta cell methylation versus age in binding sites. Median methylation values across the (a) *FOXA2* and (b) *NKX2.2* binding sites in the fifth quintile of the median methylation levels for 7 CTL (blue) and 7 T2D (red) age-matched donors.



Extended Data Fig. 9 | Pre-processing workflow. Workflow of the HPA methylation data pre-processing.

Reporting Summary

Nature Portfolio wishes to improve the reproducibility of the work that we publish. This form provides structure for consistency and transparency in reporting. For further information on Nature Portfolio policies, see our [Editorial Policies](#) and the [Editorial Policy Checklist](#).

Statistics

For all statistical analyses, confirm that the following items are present in the figure legend, table legend, main text, or Methods section.

- | n/a | Confirmed |
|-------------------------------------|--|
| <input type="checkbox"/> | <input checked="" type="checkbox"/> The exact sample size (n) for each experimental group/condition, given as a discrete number and unit of measurement |
| <input type="checkbox"/> | <input checked="" type="checkbox"/> A statement on whether measurements were taken from distinct samples or whether the same sample was measured repeatedly |
| <input type="checkbox"/> | <input checked="" type="checkbox"/> The statistical test(s) used AND whether they are one- or two-sided
<i>Only common tests should be described solely by name; describe more complex techniques in the Methods section.</i> |
| <input type="checkbox"/> | <input checked="" type="checkbox"/> A description of all covariates tested |
| <input type="checkbox"/> | <input checked="" type="checkbox"/> A description of any assumptions or corrections, such as tests of normality and adjustment for multiple comparisons |
| <input type="checkbox"/> | <input checked="" type="checkbox"/> A full description of the statistical parameters including central tendency (e.g. means) or other basic estimates (e.g. regression coefficient) AND variation (e.g. standard deviation) or associated estimates of uncertainty (e.g. confidence intervals) |
| <input type="checkbox"/> | <input checked="" type="checkbox"/> For null hypothesis testing, the test statistic (e.g. F , t , r) with confidence intervals, effect sizes, degrees of freedom and P value noted
<i>Give P values as exact values whenever suitable.</i> |
| <input checked="" type="checkbox"/> | <input type="checkbox"/> For Bayesian analysis, information on the choice of priors and Markov chain Monte Carlo settings |
| <input checked="" type="checkbox"/> | <input type="checkbox"/> For hierarchical and complex designs, identification of the appropriate level for tests and full reporting of outcomes |
| <input type="checkbox"/> | <input checked="" type="checkbox"/> Estimates of effect sizes (e.g. Cohen's d , Pearson's r), indicating how they were calculated |

Our web collection on [statistics for biologists](#) contains articles on many of the points above.

Software and code

Policy information about [availability of computer code](#)

Data collection

n/a

Data analysis

Our analyses utilized public software packages. All source/versions are provided in the Methods. Software versions are also listed here: cutadapt v4.4, bwa-meth v0.2.7, samtools v1.11 (snATAC-Seq analyses) and v1.14 (methylome analyses), sambamba v0.8.1, wgbstools v0.2.0, bedtools v2.26.0, uxm v0.1.0, R v4.2 (scRNA-Seq analyses) and v4.3.2 (methylome analyses), methylSig v1.11.0, EnrichedHeatmap v1.32.0, pheatmap v1.0.12, ggplot2 v3.5.1, PCATools v2.14.0, CellRanger v7.1.0, Seurat v4.4.0 (snATAC-Seq analyses) and v4.9.9041 (scRNA-Seq analyses), SoupX v1.6.2, scDbfFinder v1.12.0, scSorter v0.0.2, DESeq2 v1.38.1, Signac v1.7.0, bedToBam v2.30.0, BAMscale v0.0.5, bigWigMerge v2, bedGraphToBigWig v2.8, Genomica v3.0.0, GSEA v4.3.3, GREGOR v1.4.0.

For manuscripts utilizing custom algorithms or software that are central to the research but not yet described in published literature, software must be made available to editors and reviewers. We strongly encourage code deposition in a community repository (e.g. GitHub). See the Nature Portfolio [guidelines for submitting code & software](#) for further information.

Data

Policy information about [availability of data](#)

All manuscripts must include a [data availability statement](#). This statement should provide the following information, where applicable:

- Accession codes, unique identifiers, or web links for publicly available datasets
- A description of any restrictions on data availability
- For clinical datasets or third party data, please ensure that the statement adheres to our [policy](#)

Raw data and metadata related to this work are available on the PancDB website <https://hpap.pmacs.upenn.edu> and on dbGaP (<https://www.ncbi.nlm.nih.gov/gap/>) with accession phs002465 (v2). At the PancDB website Interactive Analysis link, it is also possible to explore Genome Browser tracks for our methylation data as well as the results of islet perfusion experiments utilized in our insulin secretion ratio calculations. Finally, the result files for the methylome comparisons in this work as well as the scRNA-Seq DESeq2 results are available in the Supplemental File archive.

Human research participants

Policy information about [studies involving human research participants and Sex and Gender in Research](#).

Reporting on sex and gender	Our data were from deceased human donors. Sex information was determined at the time of organ collection. We do not have gender information for these donors. Sex information is available in the Supplemental tables and at the PancDB site (https://hpap.pmacs.upenn.edu/).
Population characteristics	Donor characteristics (including age, sex, disease group, ancestry, etc.) are available in the Supplemental Tables and at the PancDB site (https://hpap.pmacs.upenn.edu/).
Recruitment	N/A
Ethics oversight	N/A, the study was considered 'exempt' by the UPenn IRB because deceased donors are not considered research participants.

Note that full information on the approval of the study protocol must also be provided in the manuscript.

Field-specific reporting

Please select the one below that is the best fit for your research. If you are not sure, read the appropriate sections before making your selection.

- Life sciences Behavioural & social sciences Ecological, evolutionary & environmental sciences

For a reference copy of the document with all sections, see [nature.com/documents/nr-reporting-summary-flat.pdf](https://www.nature.com/documents/nr-reporting-summary-flat.pdf)

Life sciences study design

All studies must disclose on these points even when the disclosure is negative.

Sample size	Several comparisons were carried out, each with specific subsets of the available samples. Sample sizes ranged from 7 to 21, depending on the comparison..
Data exclusions	Inclusion criteria for each comparison are specified in the manuscript.
Replication	Each comparison involved biological replicates.
Randomization	N/A
Blinding	N/A

Reporting for specific materials, systems and methods

We require information from authors about some types of materials, experimental systems and methods used in many studies. Here, indicate whether each material, system or method listed is relevant to your study. If you are not sure if a list item applies to your research, read the appropriate section before selecting a response.

Materials & experimental systems

- | n/a | Included in the study |
|-------------------------------------|--|
| <input checked="" type="checkbox"/> | <input type="checkbox"/> Antibodies |
| <input checked="" type="checkbox"/> | <input type="checkbox"/> Eukaryotic cell lines |
| <input checked="" type="checkbox"/> | <input type="checkbox"/> Palaeontology and archaeology |
| <input checked="" type="checkbox"/> | <input type="checkbox"/> Animals and other organisms |
| <input checked="" type="checkbox"/> | <input type="checkbox"/> Clinical data |
| <input checked="" type="checkbox"/> | <input type="checkbox"/> Dual use research of concern |

Methods

- | n/a | Included in the study |
|-------------------------------------|---|
| <input checked="" type="checkbox"/> | <input type="checkbox"/> ChIP-seq |
| <input checked="" type="checkbox"/> | <input type="checkbox"/> Flow cytometry |
| <input checked="" type="checkbox"/> | <input type="checkbox"/> MRI-based neuroimaging |